nature ecology & evolution

Article

https://doi.org/10.1038/s41559-025-02773-w

Functional replacement of ancestral antibacterial secretion system in a bacterial plant pathogen

Received: 8 November 2024

Accepted: 27 May 2025

Published online: 4 July 2025

Check for updates

Chloé Peduzzi[1], Jules Butchacas[2,3], François Nikis[1], Nathaniel Heiden[4], Marcus V. Merfa[2,3], Manon Martin[5], Veronica Roman-Reyna[6], Jonathan M. Jacobs[2,3], Ralf Koebnik[7] & Claude Bragard[1]

Two distinct molecular machineries, T4SS and T6SS, have been found within the order Xanthomonadales to be involved in outcompeting other bacterial species through the secretion of toxic effector proteins. However, the ecological and evolutionary basis leading xanthomonads to evolve two secretion systems with such similar functions remain unclear. Here we show that *Xanthomonas translucens* (*Xt*) lineages have switched from an X-T4SS-mediated to T6SS-i4-mediated bacterial killing strategy. T6SS-i4 was only found in *Xt* strains lacking X-T4SS and vice versa, resulting in a patchy distribution of the two nanoweapons along the *Xt* phylogeny. Using genetic and fluorescence-based methods, we demonstrated that X-T4SS and T6SS-i4 are crucial for interbacterial competition in *Xt*, but not *Xt* T6SS-i3. Combined comparative genetic and phylogenetic analyses further revealed that the X-T4SS gene clusters have been subject to degradation and had several loss events, while T6SS-i4 was inserted through independent gain events. Overall, this research supports the ancestral state of X-T4SS and provides new insights into the mechanisms promoting *Xt* survival within their ecological niches.

Bacteria have evolved diverse antibacterial weapons to eliminate competing organisms[1]. They have adopted none, one or a combination of these competition strategies to thrive within mixed microbial populations, whether in the gut, insect or plant microbiomes[1,2]. Bacterial secretion systems that deliver toxic effectors directly into neighbouring bacteria via contact-dependent manner appear to be widespread. Their differing structural origins and respective toxin repertoires suggest that each system confers fitness advantages. However, the ecological and evolutionary rationale for adopting one strategy over another remains unclear.

The genus *Xanthomonas* is a large group of Gram-negative plant-associated bacteria causing diseases in more than 350 host plants worldwide[3,4]. Hitherto, two distinct families of secretion systems involved in antibacterial competition are found among xanthomonads, namely T4SS[5] and T6SS[6]. Although both machineries require physical cell-to-cell contact, they differ markedly in distribution and architecture as well as for effector loading and delivery mechanisms[7,8]. Although the T4SS and T6SS effector–immunity pair repertoires appear to differ, the redundancy in some toxins sharing similar toxic domains also suggests cross-talk between systems[7,8].

[1]Applied Microbiology-Plant health, Earth & Life Institute, UCLouvain, Louvain-la-Neuve, Belgium. [2]Department of Plant Pathology, The Ohio State University, Columbus, OH, USA. [3]Infectious Diseases Institute, The Ohio State University, Columbus, OH, USA. [4]Levo International, Bloomfield, CT, USA. [5]Louvain Institute of Biomolecular Science and Technology (LIBST), UCLouvain, Louvain-la-Neuve, Belgium. [6]Department of Plant Pathology and Environmental Microbiology, Pennsylvania State University, University Park, PA, USA. [7]PHIM Plant Health Institute, University of Montpellier, IRD, Institut Agro, Montpellier, France. e-mail: claude.bragard@uclouvain.be

The T6SS is identified in 25% of sequenced proteobacteria and is widely distributed, also among plant-associated pathogens and symbionts[9]. This multiproteic complex is composed of 13 core structural components (TssA-M) and accessory elements[10]. The T6SS has a dynamic structure with a membrane complex anchored in the bacterial envelope and a base plate. The cytoplasmic tail capped by a spike is enclosed in a contractile sheath. The system releases effectors by puncturing the target cell membrane[11,12]. T6SS genesis exhibits different origins, with the base plate and tail subcomplexes structurally related to T-even phages, whereas the membrane complex shares homology with the type IVb secretion system (T4bSS)[13]. In phytobacteria, T6SSs have been classified into five phylogenetic clades (i1–i5)[10]. Clade i3 was further subdivided in subclades i3*, i3** and i3*** (ref. 10). T6SSs are widely distributed within the Xanthomonadales order, with identified representatives from clades and subclades T6SS-i1, i3*, i3**, i3*** and i4 (refs. 7,14).

A specialized T4SS was also shown to have antibacterial activity via secretion of toxic effectors[8]. First characterized in *Xanthomonas citri*, other chromosomal T4SSs have since been identified in silico, mostly among other members of the Xanthomonadales[5]. The system was accordingly called Xanthomonadales-like T4SS[8]. The X-T4SS is composed of 12 structural components (VirB1–VirB11 and VirD4), similar to class A T4SSs[8]. The secretion machinery mainly consists of the core complex, an inner membrane complex anchored in the cell envelope and an extracellular pilus[8,15,16]. The ATPase VirD4 serves as a loading site for effectors[8].

Here we used *Xanthomonas translucens* (*Xt*), a pathogen on small-grain cereals and grasses[17,18], as a model to investigate the evolution of bacterial killing secretion systems. We demonstrated a distinct distribution pattern of T6SSs and X-T4SS within *Xt*. This correlated with convergent roles of *Xt* X-T4SS and T6SS-i4 for interbacterial competition. *Xt* genomic resources have been exploited to evidence functional switches from one competition strategy to another. This work expands our current understanding on how closely related bacteria adapt their competition strategies to survive in competitive environments.

Results

X-T4SS and T6SS-i4 display mutually exclusive distributions

To explore the prevalence and distribution of T6SS and X-T4SS in *X. translucens*, 94 publicly available genome sequences were analysed for the presence of homologues of core component using SecReT6/SecReT4 HMM search and BLAST tools[19–21]. Two clusters of genes encoding for distinct T6SS clades were detected in *Xt* chromosomes. Phylogenetic analysis revealed that these clusters belong to subclade T6SS-i3*** (hereafter referred to as T6SS-i3) and to clade T6SS-i4 (ref. 10). Collectively, we observed a heterogeneous distribution of T6SS-i3, T6SS-i4 and X-T4SS gene clusters along the species phylogeny (Fig. 1). In similar analyses, no T6SS-i4 core gene was found in any of the *Xanthomonas* plasmids available at the National Center for Biotechnology Information (NCBI).

On the basis of average nucleotide identity (ANI) phylogenetic analyses, *Xt* can be classified into three clades: Xt-I, Xt-II and Xt-III[18]. Xt-I genomic group (small-grain cereals pathogens) comprises two sublineages *X. translucens* pv. *undulosa* (*Xtu*) and *X. translucens* pv. *translucens* (*Xtt*). All strains of *Xtu* harboured both T6SS-i3 and T6SS-i4, while *Xtt* strains possess T6SS-i3 and either T6SS-i4 or X-T4SS. The T6SS-i4 system was only found in *Xtt* LIN subgroup K1 (ref. 22). Additionally, all X-T4SS from ANI Xt-I group presented at least one pseudogenized gene, most commonly *virD4*. Although there are only five genomes available, all strains belonging to the Xt-II genomic group (small-grain cereals and grasses pathogens) contain both T6SS-i3 and T6SS-i4. Finally, T6SS and X-T4SS gene clusters were heterogeneous and varied in their distribution in clade Xt-III (grasses pathogens) with some containing only T6SS-i4, only X-T4SS or no T6SSs or X-T4SS cluster at all.

Interestingly, X-T4SS was present when T6SS-i4 was absent and vice versa. We hypothesize that there is a mutual exclusion between T6SS-i4 and X-T4SS, which was found in all *Xt* strain in our analysis. We find a significant negative correlation between both X-T4SS and T6SS-i4 loci (case 1—posterior mean of X-T4SS = −70.570, Markov chain Monte Carlo (MCMC) $P < 5 \times 10^{-4}$; and case 2—posterior mean of X-T4SS = −11.906, MCMC $P < 5 \times 10^{-4}$) supporting this hypothesis.

Xt T6SS-i4 is required for interbacterial competition

Since the distributions of X-T4SS and T6SS-i4 in *Xt* do not overlap, we hypothesized that these systems may play redundant roles in bacterial competition. To experimentally investigate their function, we tested how knocking out each secretion system in *Xt* strains affected their ability to kill the model bacterium *Escherichia coli* DH10B[23].

The strain *Xt* UPB513 (ANI group Xt-I) harbours both complete T6SS-i3 and i4 gene clusters. To study T6SS function, we generated single- and double-mutant strains for both T6SS clades by deleting independently either the inner tube subunit Hcp protein (Δ*hcpi3*, Δ*hcpi4* and Δ*hcpi3* Δ*hcpi4)* or part of the cluster (ΔT6SS-i3, ΔT6SS-i4 and ΔT6SS-i3 ΔT6SS-i4)[6] (Fig. 2a). Qualitative competition assays were first conducted by spreading *E. coli* DH10B cells on nutrient agar (NA) plates and dropping patches of each *Xt* UPB513 wild type (WT) or T6SS mutants. Using green fluorescent protein (GFP)-expressing *E. coli* cells, we showed that *E. coli* growth was inhibited by *Xt* UPB513 WT, Δ*hcpi3* and ΔT6SS-i3, but not by Δ*hcpi4*, Δ*hcpi3* Δ*hcpi4*, ΔT6SS-i4 and ΔT6SS-i3 ΔT6SS-i4 strains (Fig. 2b). Complementing the Δ*hcpi4* strain with the *hcpi4* gene in its original location, *Xt* UPB513 Δ*hcpi4 hcpi4*$_{Xtu}$, restored the killing activity. The absence of bacterial killing activity in both the single-mutant Δ*hcpi4* and double-mutant Δ*hcpi3* Δ*hcpi4* also indicates that Hcpi3 cannot functionally replace Hcpi4. Quantification of competition between *E. coli* Km^{r} GFP^{+} cells mixed with *Xt* UPB513 WT or T6SS mutants Spec^{r} by antibiotic selection showed that *Xt* UPB513 T6SS-i4 reduces *E. coli* survival by four orders of magnitude, while *Xt* growth remained unaffected (Fig. 2c and Extended Data Figs. 1 and 2). *E. coli* DH10B does not have a T6SS or X-T4SS. Deletions of the T6SS-i3 or T6SS-i4 had no effects on *Xanthomonas* virulence on barley or bacterial growth (Extended Data Fig. 3). Further experiments showed that *Xt* UPB513 T6SS-i4 was involved in the competition against *Pantoea agglomerans* UPB1357 and *Pseudomonas sivasensis* UPB1354 (ref. 24), two bacterial strains isolated from cereals (Extended Data Fig. 4).

Real-time monitoring of T6SS-i4 killing activity confirmed competition assay results. Figure 2d shows time-lapse series of competition between *Xt* UPB513 RFP^{+} and *E. coli* DH10B GFP^{+} in a 10:1 (*Xt*: to *E. coli*) ratio over 4 h. *Xt* UPB513 WT RFP^{+} cells encircle *E. coli* GFP^{+} cells, leading to rounding and eventual lytic death of the *E. coli* cells. Some *E. coli* bacteria were not killed, but they also did not multiply over the whole 4-h period, suggesting a bacteriostatic action of some T6SS effectors. In contrast, co-incubation with *Xt* UPB513 ΔT6SS-i4 RFP^{+} did not show any bacterial killing activity, only *E. coli* cells multiplication. The encircling of *E. coli* by *Xt* was observed even with T6SS mutants, indicating that *Xt* could detect and target *E. coli* independently of a functional T6SS. *Xt* lysis events were extremely rare (*X. translucens* WT is shown in Supplementary Videos 1–8; *X. translucens* T6SS-i4 mutant is shown in Supplementary Videos 9–16).

Xt X-T4SS shows similar bacterial killing activity

To validate our hypothesis of functional redundancy between T6SS and X-T4SS, we conducted competition assays with *Xt* LMG728 (ANI group Xt-III) possessing an intact X-T4SS gene cluster. To test whether X-T4SS is also responsible for interbacterial competition, we constructed a X-T4SS mutant lacking ATPase VirD4 protein (Δ*virD4*)[25] (Fig. 3a). Using similar qualitative and quantitative competition assays as described above, *Xt* LMG728 WT induced *E. coli* death, whereas *Xt* LMG728 Δ*virD4* did not kill its competitor (Fig. 3b). Killing activity was restored in the mutant when complemented by plasmid pSKX1::*virD4*. In these

https://doi.org/10.1038/s41559-025-02773-w

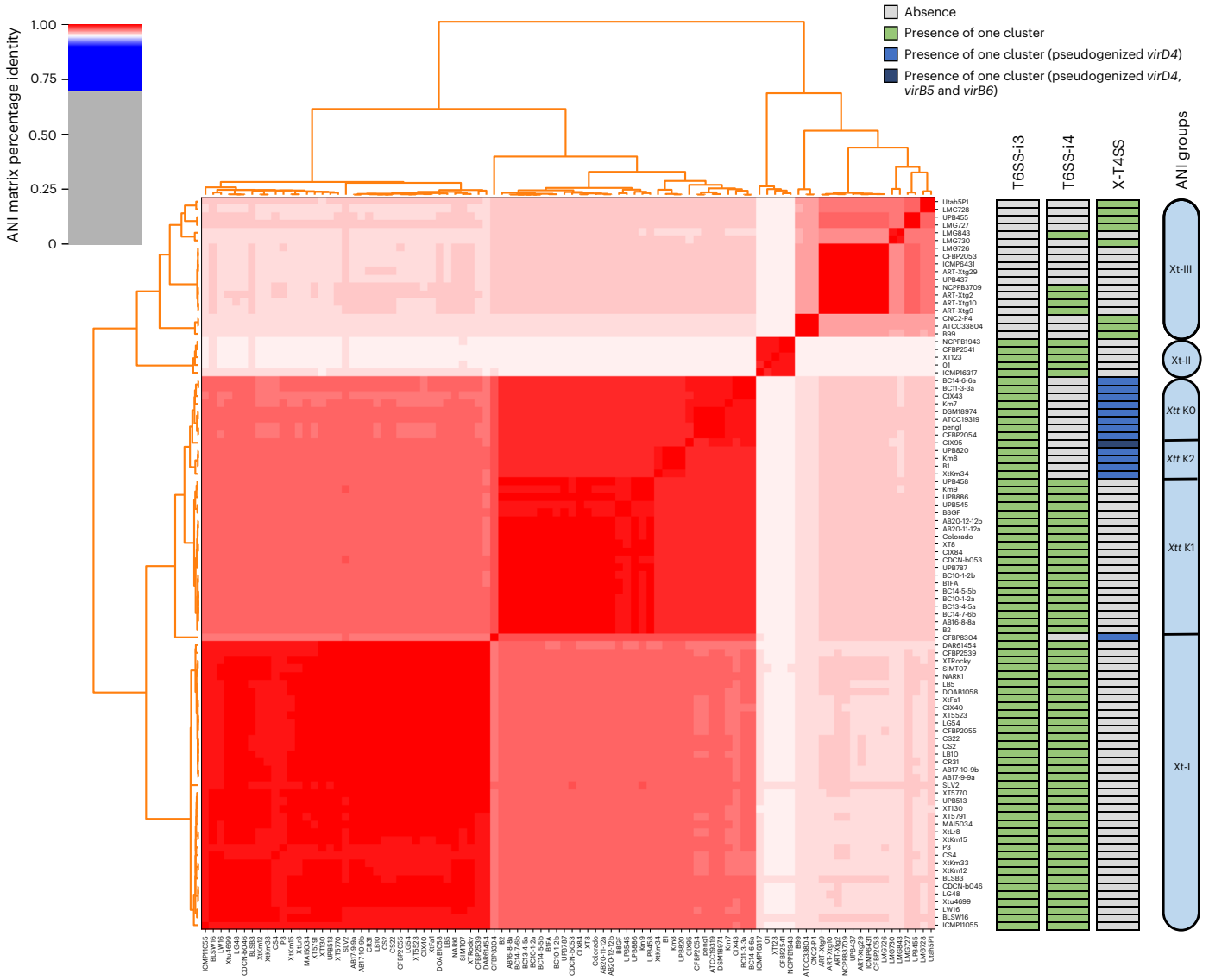

Fig. 1 | X-T4SS and T6SS-i4 show non-overlapping distribution patterns within *Xt* strains. To the left, the heatmap reflects the ANI matrix among sequenced 94 strains of the species *X. translucens*. Three columns depicted to the right of the heatmap summarize, for each strain, the presence or absence of T6SS-i3, T6SS-i4 and X-T4SS gene clusters with the following colour code: absence of gene cluster (grey), presence of gene cluster (green) or presence of gene cluster with pseudogenized genes (dark blue). Presence is based on the presence of the 13 genes (T6SS) and 12 genes (X-T4SS) for complete genomes and at least 11 genes (T6SS) and 9 genes (X-T4SS) for draft genomes. The three ANI clades Xt-I, Xt-II and Xt-III and three LIN groups within *Xtt*, as described by ref. 18 and ref. 22, respectively, are represented on the far right of this figure. Dendrograms were built with single-linkage hierarchical clustering trees based on pairwise identity matrix using Pyani[62].

competition assays, *Xt* LMG728 suppressed *E. coli* viability by four orders of magnitude, but neither *Xt* LMG728 nor the isogenic *virD4* mutant showed any detectable growth defects (Fig. 3c and Extended Data Figs. 1 and 2). Additionally, both *Xt* strains grew at comparable rates in liquid medium in vitro (Extended Data Fig. 3). Similarly to *Xt* UPB513 T6SS-i4, *Xt* LMG728 competitiveness against *P. agglomerans* UPB1357 and *Ps. sivasensis* UPB1354 (ref. 24) was X-T4SS dependent (Extended Data Fig. 4).

Taken together, these results support functional redundancy between T6SS-i4 and X-T4SS for bacterial killing in *Xt*.

X-T4SS has been acquired before *Xanthomonas* clades split

Because of their similar function, we hypothesized that the heterogeneous distribution of both systems signified functional displacement of X-T4SS by T6SS-i4 gene cluster. To test this, we combined comparative genetics and phylogenetic analyses. We screened the type or pathotype strain of each *Xanthomonas* species and pathovar for the presence of X-T4SS, including those strains in further analyses if present. A phylogenetic tree was then built on the basis of *virD4* genes, excluding pseudogenes. *Xanthomonas* species with experimentally validated X-T4SS involved in bacterial killing were also included[5], replacing the type strains of species in those cases. Our results showed that the X-T4SS gene phylogeny was mostly congruent with the species tree (Fig. 4). Exceptions have, however, been found for some *Xanthomonas* strains clustering separately from both *Xanthomonas* clade 1 and 2 groups when using other X-T4SS genes than *virD4* to construct the X-T4SS phylogenetic tree (Extended Data Fig. 5). To investigate reasons behind these different groupings, we used BLAST and found that some X-T4SS genes had higher sequence similarity to *Stenotrophomonas* X-T4SS genes, indicating X-T4SS intergenus gene exchange. Finally, we also found X-T4SS in *X. citri* strains from herbarium specimens spanning a period of >120 years in the nineteenth and twentieth centuries[26].

https://doi.org/10.1038/s41559-025-02773-w

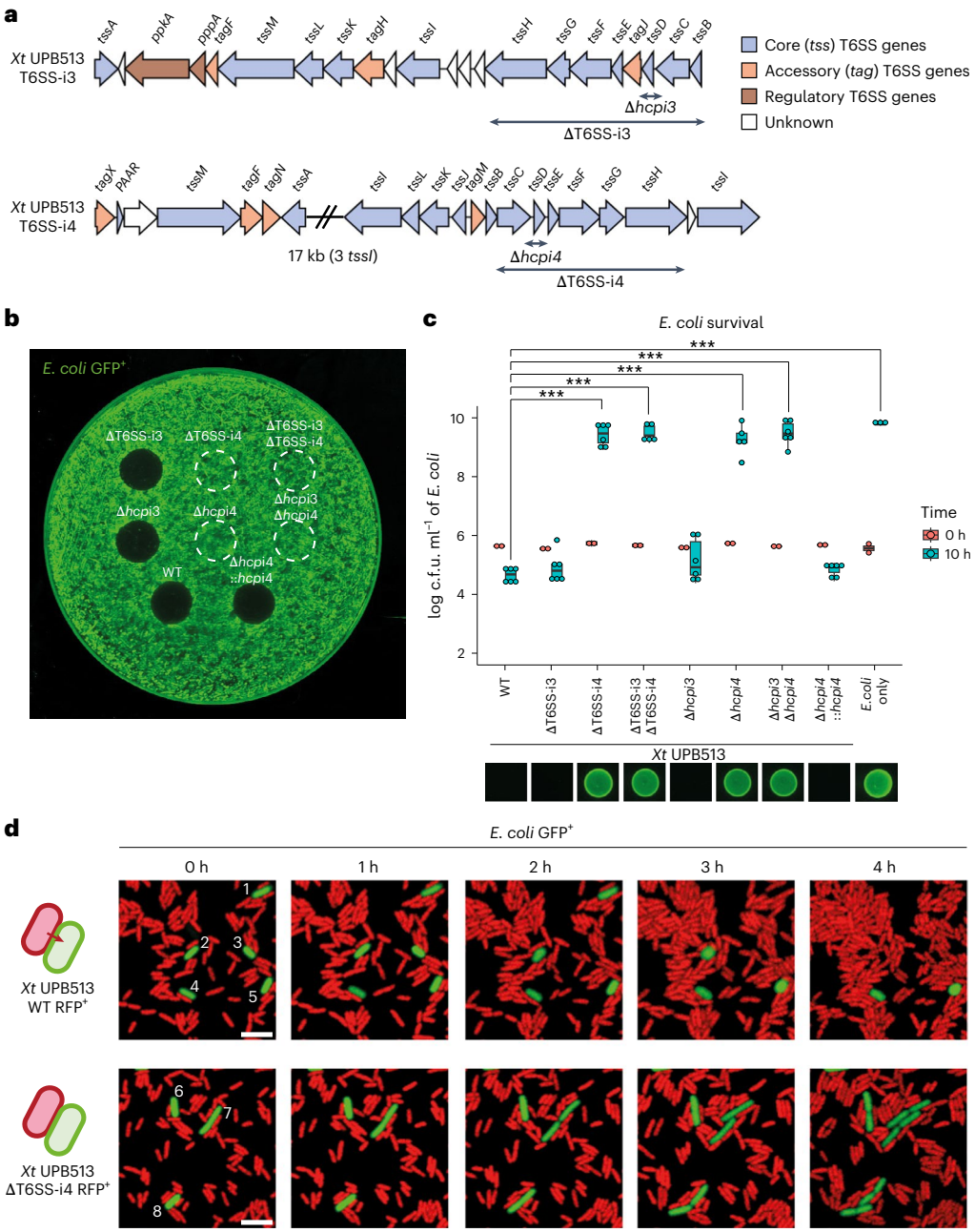

Fig. 2 | *Xt* interbacterial competition relies on T6SS-i4, but not T6SS-i3. **a**, Overview of genes deleted in the *Xt* UPB513 T6SS-i3 and T6SS-i4 gene clusters for the construction of T6SS mutant strains. **b**–**d**, Competition assays using *Xt* UPB513 WT, ΔT6SS-i3, ΔT6SS-i4, ΔT6SS-i3 ΔT6SS-i4, Δ*hcpi3*, Δ*hcpi4*, Δ*hcpi3* Δ*hcpi4* and Δ*hcpi4*::*hcpi4* as attacker cells and *E. coli* DH10B pPneo-gfp as a target cell are shown: representative qualitative assay (**b**), quantitative assay (**c**) and time lapse (**d**). **b**, Representative qualitative assay plate after 16 h of competition on NA using Amersham Typhoon laser scanner (filter Cy2 525BP20). **c**, Quantitative assay with competitors mixed in a 10:1 ratio (*Xt* to *E. coli*) for 10 h of cocultivation. Bottom, fluorescence images of representative competition patches spotted on NA after 10 h of cocultivation using Amersham Typhoon laser scanner. Top, boxplot represents *E. coli* survival log c.f.u. ml^{-1} after 0 h and 10 h of cocultivation. All boxplots show first and third quartiles around the median. Whiskers represent the smallest and largest values no further than 1.5× interquartile range (IQR) from the hinge. Dots indicate independent biological replicates ($n = 2$ at 0 h; $n = 6$ at 10 h). Significance was tested by two-sided Student's *t*-test. ***$P < 0.001$, **$P < 0.01$, *$P < 0.05$, only significant comparisons are shown (ΔT6SS-i3, $P = 1$; ΔT6SS-i4, $P = 1.47 \times 10^{-9}$; ΔT6SS-i3 ΔT6SS-i4, $P = 3.72 \times 10^{-10}$; Δ*hcpi3*, $P = 1$; Δ*hcpi4*, $P = 3.11 \times 10^{-8}$; Δ*hcpi3* Δ*hcpi4*, $P = 2.13 \times 10^{-9}$; Δ*hcpi4*::*hcpi4*, $P = 1$; and *E.coli* only, $P = 1.03 \times 10^{-11}$). **d**, Time-lapse pictures of *Xt* WT and T6SS-i4 mutant (ΔT6SS-i4), expressing RFP in competition with *E. coli* expressing GFP (1 h between frames). Top row, *E. coli* cells nos. 2 and 5 rounded up; cells nos. 1, 2 and 3 get lysed; cell no. 4 shows no cell division. Bottom row, cells nos. 6, 7 and 8 multiply over time. Both mCherry and GFP channels are merged in each image. Scale bar, 4 µm.

In line with our phylogenetic findings, all X-T4SS gene clusters shared the same chromosomal location across all *Xanthomonas* strains in this study. The *virD4* gene is consistently found downstream of the *uvrB* gene, with some genomes also possessing a transfer RNA^{Val} gene between the *uvrB* and *virD4* genes. On the other border, the neighbouring gene of X-T4SS clusters is mostly the *thrS* gene, although a few in *Xanthomonas* species are affected by genome reorganizations.

The similar X-T4SS and species tree topologies, along with the shared genomic location of X-T4SS in distantly related xanthomonads, provide evidence that X-T4SS was probably acquired before the

https://doi.org/10.1038/s41559-025-02773-w

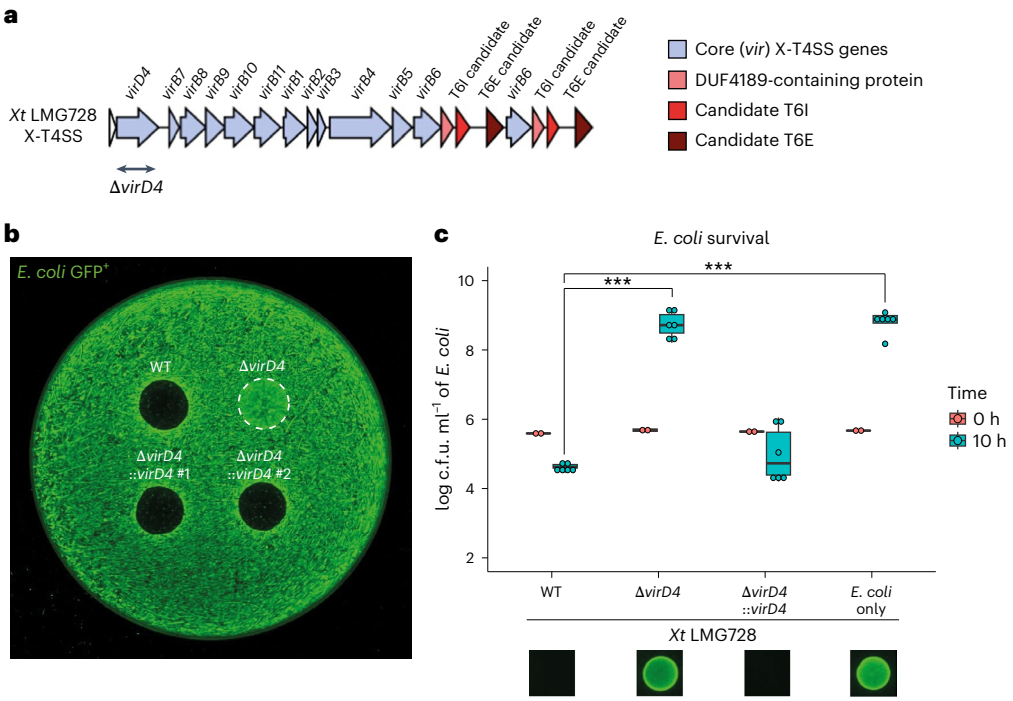

Fig. 3 | *Xt* X-T4SS is crucial for interbacterial competition. a, Overview of genes deleted in the *Xt* LMG728 X-T4SS gene cluster for the construction of the X-T4SS mutant strain. **b**,**c**, Competition assays using *Xt* LMG728 WT, Δ*virD4* and Δ*virD4* pSKX1::*virD4* as attacker cells and *E. coli* DH10B pPneo-gfp as a target cell are shown: representative qualitative assay (**b**) and quantitative assay (**c**). **b**, Representative qualitative assay plate after 16 h of cocultivation on NA using Amersham Typhoon laser scanner (filter Cy2 525BP20). **c**, Quantitative assay with competitors mixed in a 10:1 ratio (*Xt to E. coli*) for 10 h of cocultivation. Bottom, fluorescence images of representative competition patches spotted on NA after 10 h of cocultivation using Amersham Typhoon laser scanner. Top, boxplot represents *E. coli* survival log c.f.u. ml^{-1} after 0 and 10 h of cocultivation. All boxplots show first and third quartiles around the median. Whiskers represent the smallest and largest values no further than 1.5× IQR from the hinge. Dots indicate independent biological replicates ($n = 2$ at 0 h; $n = 6$ at 10 h). Significance was tested by two-sided Student's *t*-test. ***$P < 0.001$), **$P < 0.01$), *$P < 0.05$), only significant comparisons are shown (Δ*virD4*, $P = 5.86 \times 10^{-10}$; Δ*virD4*::*virD4*, $P = 0.86$; and *E.coli* only, $P = 1.22 \times 10^{-10}$).

split of *Xanthomonas* clades 1 and 2, which may have occurred ~100 to 200 million years ago, and then vertically inherited in the progeny of *Xanthomonas* sp.

Ancestral X-T4SS clusters have been subjected to loss events

To further explore the X-T4SS evolutionary history, we compared X-T4SS clusters and neighbourhood between representative strains of each *Xt* ANI clade, along with the corresponding regions in X-T4SS-lacking strains (Extended Data Fig. 6). Comparison of X-T4SS clusters first revealed that all X-T4SS in *Xt* are well conserved in terms of genetic organization. All *virD4* genes in *Xt* strains from ANI group I were pseudogenized due to frameshift mutations and internal stop codons caused by a nucleotide deletion (Supplementary Fig. 1). Accordingly, fragments of the *virB6* gene were found in the corresponding location of X-T4SS-lacking *Xt* strains, indicating these X-T4SS clusters have been in the process of decay or subjected to loss events. Pseudogenes and gene fragments were also common in other *Xanthomonas* species. This indicates a convergent loss of X-T4SS caused by different mechanisms such as IS insertion or indel mutations identified in this study. Additionally, screening for X-T4SS effector XVIPCD motif based on HMM profiles revealed the presence of X-T4SS effectors–immunity pairs in *Xt* strains lacking X-T4SS. Some X-T4SS effectors in X-T4SS-deficient strains have been pseudogenized, while retaining an intact immunity protein, as exemplified by *Xt* UPB513 T6SS-i4$^+$ (Extended Data Fig. 7).

Horizontal gene transfer drove the evolution of T6SS-i4

To better understand the evolution of T6SS-i4, we conducted similar analyses using the well-conserved sheath subunit *tssC* gene to construct the phylogenetic tree and trace the evolutionary history of T6SS-i4 among *Xanthomonas* species. The T6SS-i4 gene phylogeny was not congruent with the species tree, suggesting that the system experienced independent horizontal gene transfer events during evolution (Fig. 5). Specifically, *Xt* ANI groups Xt-I, Xt-II and Xt-III clustered separately. For instance, *Xt* pvs. *phleipratensis* and *graminis* (ANI group Xt-III) grouped together with *X. bromi*, a bromegrass pathogen. Phylogenetic analyses were further performed among different *Xt* strains by concatenating T6SS-i4 core genes. Incongruences between the *Xt* species tree and T6SS-i4 phylogenies were also noted within the same *Xt* ANI group, as seen with strains *Xt* LW16 and BLSW16 (Extended Data Fig. 8). The incongruence was resolved in the phylogeny without *tssM* gene, where *Xt* LW16 and BLSW16 clustered with other *Xtu* strains, similar to the species tree. A similar pattern was observed for the *tssB* gene with strains XT5523 and CFBP 2055. These instances suggest potential intraspecies T6SS gene exchanges from *Xtt* to *Xtu*.

T6SS-i4 clusters were found at different genomic locations in different *Xanthomonas* lineages. Across all analysed strains, T6SS-i4 was found in seven distinct genomic locations, with *Xt* T6SS-i4 present in four of them (Supplementary Figs. 2 and 3). For each of the four neighbouring regions of *Xt*, we compared T6SS-i4 clusters between representative strains of each *Xt* ANI clade, and the corresponding region in T6SS-i4-lacking strains (Supplementary Figs. 4–7). The comparison showed a conserved genetic organization, except for a variable region of 13–64 kb that splits *Xt* T6SS-i4 into two subregions. Some upstream genes were conserved regardless of the neighbourhood type and may regulate the system or represent potential effectors–immunity pairs. Within xanthomonads, two strains in our study had their two T6SS subregions separated by more than 2 megabases (Mb)

https://doi.org/10.1038/s41559-025-02773-w

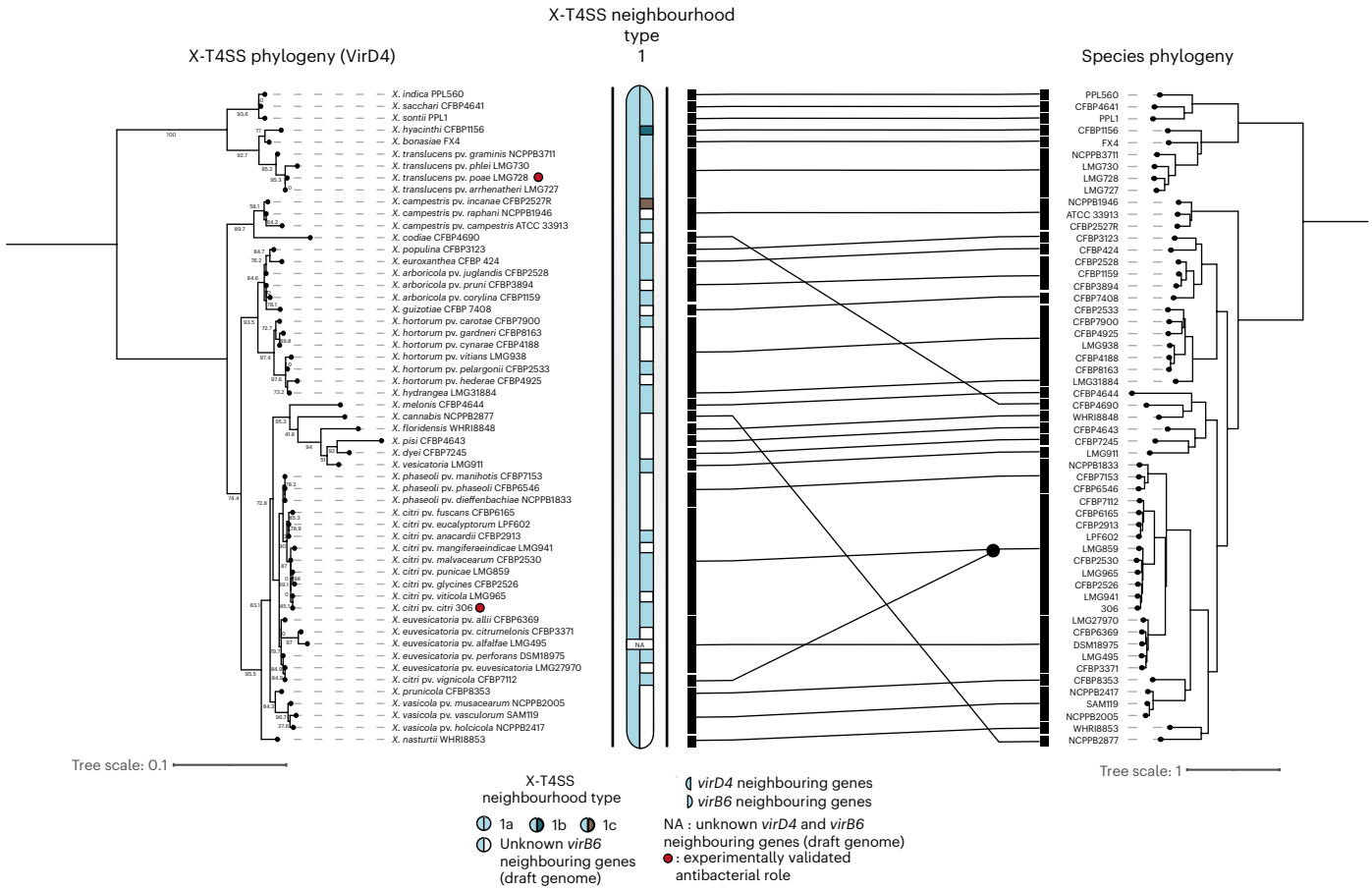

Fig. 4 | X-T4SS gene phylogeny is congruent with the species tree. Tanglegram comparing VirD4 based X-T4SS phylogeny (left) with a kSNP3-based species phylogeny (right). The X-T4SS tree was inferred by maximum likelihood using IQ-TREE based on encoded amino acid sequences of *virD4* genes aligned by ClustalW. The species pan-genome single nucleotide polymorphism (SNP)-based tree was constructed with *Xanthomonas* genomes using kSNP3 (*k*-mer of 21 bp). Trees are midpoint rooted and visualized with iTOL. Neighbourhood regions associated with each X-T4SS gene cluster are indicated next to the X-T4SS phylogenetic tree. T4SSs whose antibacterial effect have been experimentally validated are indicated next to the corresponding strain (LMG728, 306)[5].

in distinct regions of the genome, *X. oryzae* (*Xo*) NCPPB 4346 and *Xo* PXO99. The type-2 neighbourhood was the most common insertion site for T6SS-i4 in the *Xanthomonas* genus (Fig. 5). These results led us to conclude that T6SS-i4 has been horizontally transferred several times during xanthomonads evolution.

ICE mechanisms are involved in T6SS-i4 distribution

To better understand the distribution of T6SS-i4 within the *Xanthomonas* genus, we investigated potential transfer mechanisms. In the type-2 neighbourhood, genes annotated as 'prophage integrase' (*intS*) and tRNA gene were found just upstream of the T6SS-i4 cluster. IslandViewer4 confirmed the presence of genomic islands (GIs) with typical features[27–29] (Supplementary Fig. 8). The GIs containing the T6SS-i4 cluster are 150–200 kilobases (kb) in size, have lower G + C content, which differs from the rest of the genome, and include an integrase for insertion and excision, and several IS elements. These islands are inserted at a $tRNA^{Gly}$ gene and flanked by 16-base pair (bp) perfect direct repeats (DR) corresponding to attachment core sites of *attL* and *attR*. The same DR sequence was found in related strains lacking the T6SS-i4, corresponding to the *attP* integration site. However, in some T6SS-i4-deficient strains, other mobile genetic elements, including conjugative T4SS genes, were integrated at the same genomic location instead, indicating integrative and conjugative elements (ICEs) insertion (Extended Data Fig. 9). Some strains even possess a GI insertion containing the T6SS-i4 cluster followed by a tandem ICE insertion, flanked by similar DRs. This indicates that T6SS-i4 gene clusters might be *cis*-mobilizable elements (CIMEs) transferred in *cis* by the ICE to a recipient cell. In some lineages, an IS3 transposase truncated the *intS* gene, potentially fixing the antibacterial trait by preventing GI excision.

X-T4SS and T6SS-i4 effector arsenals in *Xanthomonas*

To compare the effector arsenals of X-T4SS and T6SS-i4, we analysed four pairs of genetically close *Xanthomonas* strains carrying either system. Various candidate T6SS effectors could be identified associated with diverse putative toxic domains, including Tox-URI2 DNase, phospholipase effector Tle1-like, T6SS effector BTH, chitinase and Ntox15 nuclease (Supplementary Tables 1–3). Similarly, many candidate X-T4SS effectors were predicted with potential toxic domains, such as Zeta toxin, fungal lipase and cell wall hydrolases (Supplementary Tables 1–3). Many candidate effectors also showed no match to known domains. Overall, both X-T4SS and T6SS-i4 possess a broad diversity of antibacterial toxin activities.

No T6SS-i4 effectors were detected in the four T6SS-i4 lacking strains. In contrast, X-T4SS effectors were found in both X-T4SS-containing and X-T4SS-lacking strains, although degradation mechanisms (frameshifts, deletions or IS element insertions) were observed. Strains lacking X-T4SS also had fewer X-T4SS effectors than their genetically close X-T4SS-containing strain. The X-T4SS effector degradation, along with the exclusive presence of T6SS-i4 effectors in T6SS-i4-possessing strains, support the switch from X-T4SS- to T6SS-i4-mediated bacterial killing strategy in xanthomonads.

https://doi.org/10.1038/s41559-025-02773-w

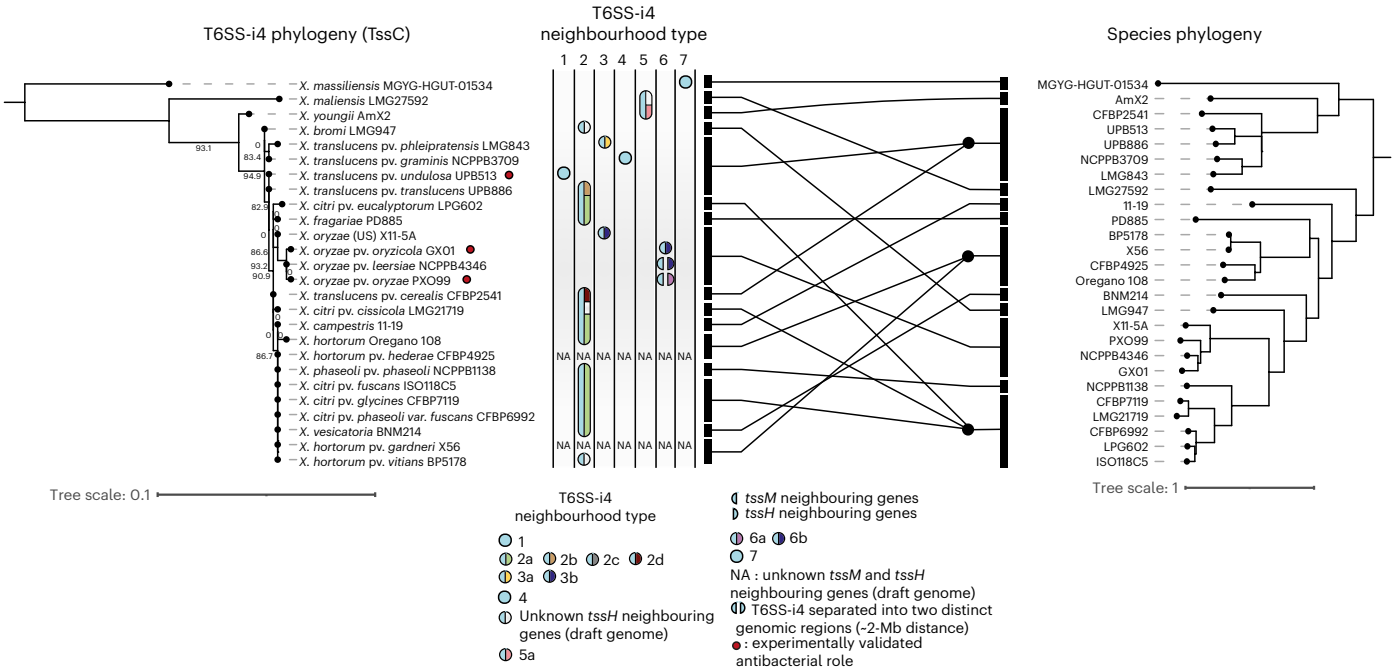

Fig. 5 | T6SS-i4 gene phylogeny is not congruent with the species tree. Tanglegram comparing TssC-based T6SS-i4 phylogeny (left) with a kSNP3-based species phylogeny (right). The T6SS-i4 tree was inferred by maximum likelihood using IQ-TREE based on encoded amino acid sequences of *tssC* genes aligned by ClustalW. The species pan-genome SNP-based tree was constructed with *Xanthomonas* strain genomes using kSNP3 (*k*-mer of 23 bp). Trees are midpoint rooted and visualized with iTOL. Neighbourhood regions associated with each T6SS-i4 gene cluster are indicated next to the T6SS-i4 phylogenetic tree. T6SS-i4 whose antibacterial effect have been experimentally validated are indicated next to the corresponding strain name (UPB513, GX01, PXO99)[6,30].

Discussion

Antibacterial weapons have arisen several times in bacteria, with xanthomonads adopting two competitive strategies depending on their lineage: X-T4SS or T6SS. Here we demonstrate that *Xt* X-T4SS and T6SS-i4 have overlapping bacterial killing activities. Our functional study on both *Xt* T6SS-i4 and X-T4SS aligns with previous findings in the Xanthomonadales order. T6SS-i4 has been shown to mediate bacterial competition in *X. oryzae* pvs. *oryzae*[30] and *oryzicola*[6] (*Xoo* and *Xoc*) and *Stenotrophomonas rhizophila*[31]. Similarly, X-T4SS-mediated killing was demonstrated in three genera: *X. citri*[5], *Stenotrophomonas maltophilia*[25] and *Lysobacter enzymogenes*[32,33], targeting Gram-negative bacteria and/or fungi.

Our results also indicate that X-T4SS and T6SS-i4 have mutually exclusive distributions in xanthomonads. This finding underscores the ecological importance of contact-dependent competition in *Xanthomonas*. Consistent with ref. 14, pseudogenized X-T4SS genes suggest that the system lost its function in some strains. Interestingly, some strains in this study carried X-T4SS with a mutated *virD4*, while the rest of the X-T4SS cluster genes remained intact. If the absence of VirD4 predicts for a loss of bacterial killing function, it also raises the question of whether the development of a T4SS pilus is still possible[34]. This type of surface structure does not require VirD4 and could suggest a switch to new biological functions (target cell adhesion, cell motility and so on). Finally, phylogenetic and comparative genomic analyses revealed non-orthologous genes displacement of ancestral bacterial killing X-T4SS by a T6SS-i4 competitive strategy in many *Xanthomonas* lineages.

The concept of mutual exclusion applies from the gene level to entire organism communities[35–37]. The mutual exclusion of X-T4SS and T6SS-i4 could be due to several factors: functional redundancy leading to the replacement of one by the other, energy costs for maintaining both systems or space constraints for both machineries in the cell envelope. This is especially relevant as both systems appear to be constitutively expressed in culture media[14]. X-T4SS homeostasis is controlled by the repressor CsrA, which maintains a constant density of X-T4SS in the cell envelope[38]. For T6SS-i4, future studies are needed to clarify how *Xanthomonas* balances the energy costs and competitive advantages, and on a possible TagF-mediated regulatory mechanism[6,7]. However, even if the loss of a redundant secretion system that is no longer needed could have an evolutionary benefit, it should be kept in mind that most bacteria use several secretion systems and sometimes many copies of the same one. Therefore, the role of energy costs in minimizing secretion potential is not yet clear. While this mutual exclusion generally holds true for the *Xanthomonas* genus, exceptions exist, such as *Lysobacter gummosus* 3.2.11 (refs. 7,8), *L. enzymogenes* C3 (refs. 7,8), some *X. citri* (for example, ISO118C5, CFBP 7119 and CFBP 6992) and *X. phaseoli* (for example, NCPPB 1138). In *Pectobacterium*, both T4SS and T6SS, evolutionarily distant from the X-T4SS and T6SS of *Xanthomonas*, redundantly secrete effectors to drive bacterial competition[39].

The loss of ancestral X-T4SS in many *Xanthomonas* species and the acquisition of the T6SS-i4 by horizontal gene transfer (HGT) only in restricted lineages result from two possible scenarios (Fig. 6), either arrival of T6SS-i4 triggered X-T4SS loss or the presence of X-T4SS, prevented the acquisition of T6SS-i4. The decay of X-T4SS occurring independently of T6SS-i4 presence is in favour of the second scenario.

Finally, we propose several ecological reasons for adopting one system over the other. First, each system may provide distinct evolutionary advantages in different microbiome contexts or co-evolving with T6SS-i4 competitors. In line with a recent study, the clustering of both *Xt* (ANI group Xt-III) and *X. bromi* T6SS-i4 suggests HGT events[40]. Occupying similar niches, this shared competitive trait is probably linked to microbiome adaptation. Second, the distribution of X-T4SS, restricted to Xanthomonadales, differs markedly from the more widespread T6SS in Proteobacteria. The uniqueness of X-T4SS might confer evolutionary advantages due to the seldom occurrence of its effector–immunity sets, while T6SS displays higher diversity in effector–immunity pairs among various Gram-negative bacteria, facilitating transfer and recombination possibilities between effector modules[41].

https://doi.org/10.1038/s41559-025-02773-w

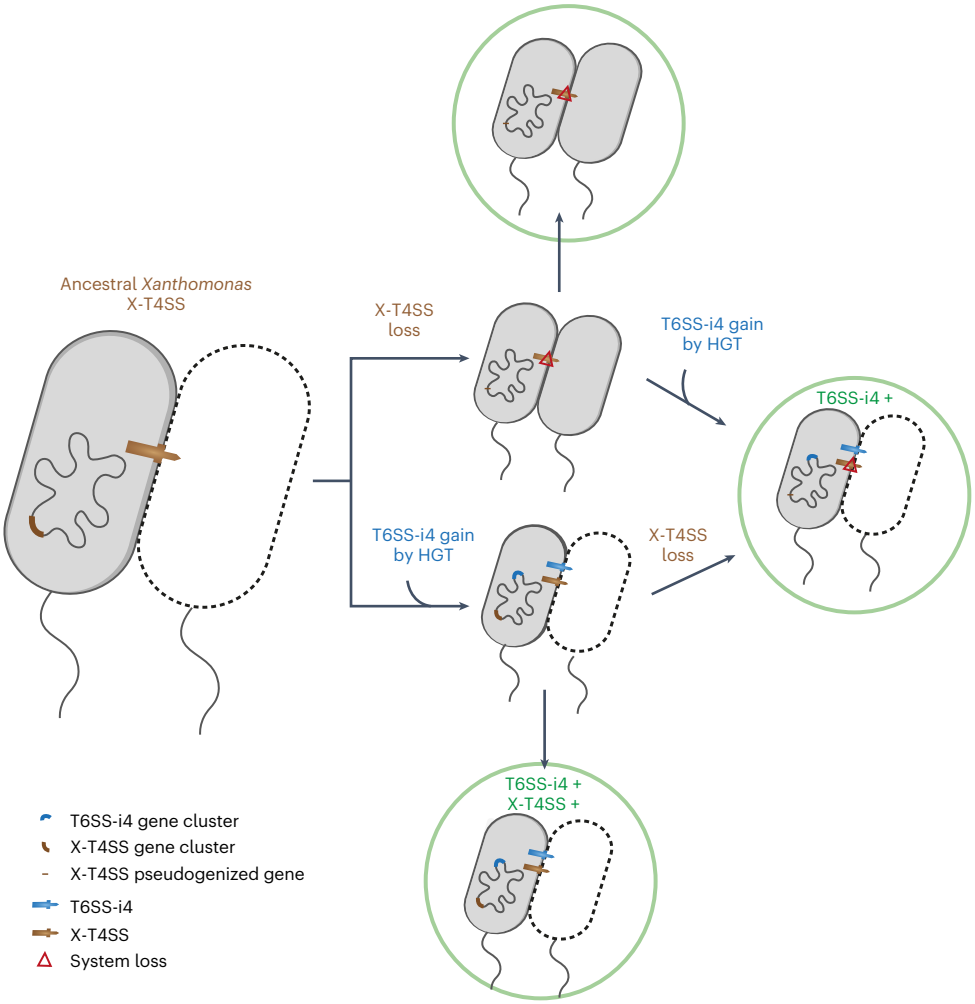

Fig. 6 | Evolutionary scenarios explaining X-T4SS loss, T6SS-i4 gain and resulting mutual exclusion profiles in xanthomonads. Our competition assays and phylogenetic analyses support an evolutionary model in which the loss of the ancestral X-T4SS and the gain of T6SS-i4 result from two possible scenarios, either by the introduction of T6SS-i4 driving X-T4SS loss, or by the presence of X-T4SS preventing the acquisition of T6SS-i4.

At this point, based on sequence comparisons, we have no indication of recruitment of X-T4SS toxins by alternative secretion systems in X-T4SS-lacking strains.

It remains unknown how easily target bacteria can evolve resistance to such contact-dependent bactericidal systems and whether the frequency of X-T4SS- and T6SS-resistant bacteria is different, which could explain the functional replacement of one system by another. For T6SS, in vitro work on *E. coli*, *Vibrio cholerae* and *Bacteroides fragilis* refute the postulate that T6SS is energetically costly[42–44]. In addition, production of X-T4SS by *X. citri* was shown to impose a notable physiological cost to the cell[38]. The loss of X-T4SS might result from increased fitness through reduced energy costs or switch to a new biological function with T4SS pilus, while retaining immunity molecules of interest[45]. Both X-T4SS and T6SS have overlapping roles in bacterial killing, but they may also perform additional functions, such as secreting antifungal effectors such as those in *L. enzymogenes* X-T4SS[32,33], or mediating specific interspecies or intraspecies competition, which could provide a fitness advantage. T6SS effectors with chitinase domain and X-T4SS effectors with a fungal lipase domain were identified in *Xanthomonas* strains, suggesting potential antifungal activity. It would be worth investigating more attacker and target strain combinations and different environmental conditions, to further support the redundancy of the two systems.

Geographical differences in T6SS availability may also influence its distribution[45]. Previous studies have examined various ecological characteristics to explain the presence or absence of T6SS in *Xanthomonas*, but no correlation with vascularity, host range or pathogenic status was found[40]. For instance, both vascular *Xtt* and non-vascular *Xtu*, as well as vascular *Xoo* and non-vascular *Xoc*, all possess T6SS-i4 (ref. 46).

The type-2 neighbourhood region of T6SS-i4 is a hotspot for ICEs insertion well conserved among xanthomonads, with prior reports in *X. arboricola* pv. *juglandis* CFBP 7179 (Xaj-ICE)[47] and *X. campestris* CN03 (ICEXca2)[48]. Therefore, the turnover between X-T4SS and T6SS-i4 could also be explained by an incompatible genetic background that hinders T6SS-i4 acquisition, such as an ICE exclusion due to unavailable integration sites or restriction modification systems[45,49]. The transfer of T6SS by ICE raises questions about the compatibility of competition and conjugation processes[50]. However, T6SSs have been found on various conjugative platforms, including plasmids that regulate T6SS-i4 activity during conjugation, suggesting that similar mechanisms may transfer T6SS-i4-encoding CIME–ICE structures[50,51]. To date, T6SS transfer by ICE has only been reported in the Bacteroides phylum[52]. Analyses of other neighbourhoods did not reveal the presence of ICE, indicating that alternative transfer mechanisms may be at play.

Our work highlights the role of X-T4SS or T6SS as antibacterial weapons for *Xt*, but also the evolutionary history of two antibacterial

mechanisms in bacteria, enhancing our understanding of their ecological role and potential evolutionary trajectories.

Methods

In silico screening for T6SSs and X-T4SS gene clusters

To obtain a comprehensive genomic dataset for assessing the evolution of *Xt* T6SS and X-T4SS, a total of 94 *Xt* genomic sequences were retrieved from the NCBI database in January 2023.

T6SSs were predicted by combining both HMM searches and BLAST tools[19–21]. T6SS gene clusters were first detected using SecReT6 HMM search program with default parameter values (*e*-value threshold <0.0001; BLAST identity threshold for T6SS prediction >30%; BLAST Ha-value threshold for T6SS-related protein prediction >0.42), counting a maximum interval between two colocalized T6SS components of 15,000 bp and a minimum of three T6SS component proteins for each T6SS region was considered. Since only T6SS clades i3 and i4 were found in SecReT6 results, the 13 core genes from three *Xanthomonas* experimentally validated T6SS clades i3* (*X. citri* strain 306)[53], i3*** (*X. oryzae* strain PXO99)[54] and i4 (*X. oryzae* strain GX01)[6], were used as baits for further confirming the predicted T6SS loci using TBLASTN (*e*-value threshold <0.000001; BLAST identity threshold >50%). The core genes within each cluster were then carefully manually inspected. X-T4SS predictions were made similarly with SecReT4 and baiting with the 12 core genes from the characterized X-T4SS (*X. citri* strain 306)[5].

Prediction of the presence of X-T4SS and T6SS-i4 was then performed by TBLASTN analysis against the entire database of *Xanthomonas* complete and draft genomes from NCBI. The amino acid sequences of the VirB7 protein (X-T4SS) and the two proteins TssB and TssA (T6SS-i4) were used as queries, since the two left and right regions of T6SS-i4 are often found on different contigs in the case of draft genomes. The type strain of each *Xanthomonas* species or pathovar when applicable was then further screened for the 13 core genes of T6SS-i4 and 12 core genes of X-T4SS and selected for subsequent phylogenetic and comparative genomic analyses.

Bacterial strains and growth conditions

Bacterial strains, plasmids and primers used in this study are listed in Supplementary Tables 4 and 5. *Xt* strains were grown at 28 °C with shaking at 220 rounds per minute (rpm) in liquid nutrient broth (NB) or on solid NA. *E. coli* DH10B and WM3064 strains were grown at 37 °C with shaking at 220 rpm in liquid lysogenic broth (LB) or on solid LB agar (1.5%). *P. agglomerans* UPB1357 and *Ps. sivasensis* UPB135424 were grown at 28 °C on solid nutrient agar (NA). The antibiotics kanamycin (Km), spectinomycin (Spec) and gentamycin (Gm) were used in a concentration of 50, 40 and 10 μg ml^{-1}, respectively, when appropriate.

DNA manipulations

Total genomic and plasmid DNA were extracted using Wizard Genomic DNA Purification Kit (Promega) and QIAprep Spin Miniprep Kit (Qiagen). Fasta and faa files of *Xt* UPB513 (RefSeq: NZ_CP096570.1) and *Xt* LMG728 (RefSeq: NZ_CP076250.1) genomes were downloaded from NCBI. Primers were designed using Benchling (https://benchling.com). To construct the single-deletion mutants *Xtu* UPB513 ΔT6SS-i3 (MZO50_RS16930–MZO50_RS16895), ΔT6SS-i4 (MZO50_RS09125–MZO50_RS09150), Δ*hcpi3* (MZO50_RS16920) and Δ*hcpi4* (MZO50_RS09130), the upstream and downstream regions were amplified using, respectively, the primers pairs UPB513 T6SS-i3 up F/R and T6SS-i3 down F/R; T6SS-i4 up F/R and T6SS-i4 down F/R; Hcpi3 up F/R and Hcpi3 down F/R; Hcpi4 up F/R and Hcpi4 down F/R and purified using QIAquick PCR & Gel Cleanup Kit. Upstream and downstream fragments of each construct were then cloned into the digested pK18mobsacB[55] at HindIII restriction site by Gibson Assembly (New England Biolabs). Each construct was transformed into *Xtu* UPB513 by electroporation at 2.5 kV. The first genomic recombination event was selected on NA + Km and screened for sucrose sensitivity. The second recombination event was selected on NA 10% sucrose and screened for Km sensitivity. Resulting deletion mutants were confirmed by polymerase chain reaction (PCR).

Double-deletion mutants were generated by introducing pK18mobsacB::*hcpi4* and pK18mobsacB::T6SS-i3 in *Xtu* UPB513 Δ*hcpi3* and *Xtu* UPB513 ΔT6SS-i4, respectively, using the same method. To complement *Xtu* UPB513 Δ*hcpi4*, a 1,567-bp DNA fragment including the *hcpi4* coding region with its upstream and downstream regions was amplified using primers Hcpi4 up F and Hcpi4 down R. The amplicon was then cloned into the pK18mobsacB. A similar method of double-recombination events was then followed as above.

The *Xt* LMG728 Δ*virD4* (KM539_RS13635) strain was generated by amplifying the upstream and downstream regions of the *virD4* gene with the LMG728 VirD4 up F/R and VirD4 down F/R primers and cloning them into pK18mobsacB and then following the same double-recombination method, except that the plasmid was delivered into *Xt* by biparental conjugation with *E. coli* strain auxotrophic WM3064. The pSKX1::*virD4* Gm^+ for complementation was synthesized by GenScript and introduced similarly in *Xt* LMG728 Δ*virD4* by conjugation by selection on NA + Gm^+ and confirmed by PCR.

For generation of red fluorescent protein (RFP)-expressing strains, the protocol of ref. 56 was adapted to *Xt* using the mini-Tn*7* delivery system to insert a single copy of a gene into *Xt* chromosome at Tn*7* attachment (*att*Tn*7*) sites, close to *glmS* gene. This involves the cotransformation of *Xt* strain with the recombinant mini-Tn*7* vector and a helper plasmid pTNS3 encoding transposition pathway genes, followed by selection on media supplemented with antibiotics. *Xt* UPB513 WT as well as each T6SS mutant and complemented strains were transformed with Tn*7*::*mCherry* $Spec^+$ by electroporation.

Bacterial competition assays

Xt UPB513 $T6SS^+$ and LMG728 $X\text{-}T4SS^+$ WT strains and respective mutant strains, as well as *E. coli* DH10B Km^+ GFP^+, *P. agglomerans* UPB1357 and *Ps. sivasensis* UPB135424 Gm^+ GFP^+ were grown on solid media and resuspended to optical density OD_{600} = 0.5 in 10 mM $MgCl_2$. In qualitative competition assays, 100 μl of *E. coli* suspension was spread all over an NA plate using glass beads, then 15 μl of *Xt* WT and X-T4SS or T6SS mutant suspensions were dropped on the dried plate. Plates were incubated for 16 h at 28 °C. In quantitative competition assays, each *Xt* strain was mixed with *E. coli* in a ratio of 10:1 (*Xt* to *E. coli*). The 5-μl patches of each mix were dropped on NA plates and incubated for 10 h of competition at 28 °C. Patches were resuspended in 500 μl of 10 mM $MgCl_2$ and serial dilutions were plated on NA + Km plates for quantifying *E. coli* surviving cells after 0 and 10 h. Qualitative and quantitative assays were repeated at least three times with two to six replicates. *Xt* cells growth was quantified once on the basis of antibiotic selection on NA + Spec or colony cell morphology after 0 and 10 h with two to six replicates. Qualitative competition assays, quantitative competition patches and dilution plates were scanned for fluorescence using Amersham Typhoon laser scanner (filter Cy2 525BP20).

Phenotypic analyses. Pathogenicity assays were conducted by needleless inoculation of barley cv. Hercule leaves (2 weeks old) with *Xt* UPB513 WT, ΔT6SS-i3, ΔT6SS-i4 and 10 mM $MgCl_2$ as a negative control. Each strain was grown on NA and resuspended to OD_{600} = 0.01 in 10 mM $MgCl_2$. The assay was repeated twice with eight plants inoculated by treatment. Plants were placed in greenhouse conditions at 28 °C and 70% relative humidity. Growth of *Xt* WT, X-T4SS and T6SS mutants was monitored in vitro in liquid NB. Initial OD_{600} of *Xt* suspensions was adjusted to 0.001. Each treatment was performed in duplicate, from which eight subreplicates were transferred in 96-well plates and coated with Breathe-Easy sealing membrane (Diversified Biotech BEM-1). Measurements of OD_{595} were taken every 45 min during 72 h, with continuous shaking (11 Hz, 3 mm) at 28 °C using a microplate reader (Multiskan FC).

Statistical analysis

Quantitative competition data were computed in *R*. Normality of log-transformed data was tested using Shapiro–Wilk test. Statistical analyses were performed using analysis of variance ANOVA1 and Tukey post hoc multiple tests for pairwise comparison of means of each group. ANOVA1 with $P = 0.05$ was considered. Significance was tested by Student's *t*-test and *P*-value adjustment: $^{***}P < 0.001$, $^{**}P < 0.01$, $^{*}P < 0.05$.

Mutual exclusivity statistical significance. To confirm mutual exclusion between X-T4SS and T6SS-i4 loci, a series of statistical tests were run. Contingency and frequency tables for the presence and absence of X-T4SS and T6SS-i4 within the 94 *Xt* strains were calculated, considering two possible scenarios: (case 1) X-T4SS containing pseudogenes is considered as present; (case 2) X-T4SS containing pseudogenes is considered as absent.

First, a one-sided Fisher's exact test was applied to the contingency tables with the alternative hypothesis that true odds ratio is <1.

Second, Bayesian phylogenetic generalized linear mixed models were run using the R package MCMCglmm (v.2.36)[57]. UPGMA phylogenetic tree was computed on the basis of ANI distance matrix between the 94 *Xt* strains and used as a random effect. FastANI (v.1.3)[58], as implemented in Galaxy (v.23.1.4.dev0)[59], was used to calculate pairwise genome-wide nucleotide identities. A derived distance matrix was used by MEGA (v.11.0.13)[60] to construct an UPGMA phylogenetic tree[61]. We tested the effect of the presence of X-T4SS loci to explain the presence of T6SS-i4 loci given random distribution across phylogeny by running two MCMCglmm models. A first model (mod_mcmc_0) was run explaining the presence of T6SS-i4 loci as a function of phylogeny as a random effect alone. This first model was then compared to a second model (mod_mcmc_1) that explains the presence of T6SS-i4 loci as a function of phylogeny as a random effect and the presence of X-T4SS loci as a fixed effect. For both case 1 and 2, we chose the model that minimizes the deviance information criteria and best explains the response.

Confocal microscopy time-lapse videos

For real-time visualization of T6SS-i4 killing activity, time-lapse videos were recorded by laser scanning confocal microscopy using an Olympus Life Science FluoView FV3000. *Xt* UPB513 WT and T6SS mutants RFP^+ $Spec^+$ strains, as well as *E. coli* DH10B Km^+ GFP^+ were grown on solid media with appropriate antibiotics and resuspended to $OD_{600} = 1$ in distilled H_2O. Bacterial suspensions were mixed in a 10:1 (*Xt* to *E. coli*) ratio. A total of 6 µl of this solution mix was deposited on an agarose pad (25% LB, 1% agarose), then left to dry. The whole assembly was placed in a humid chamber to prevent the agarose pad from desiccating. Each time-lapse video was started after 1 h of incubation at room temperature and taken every 6 min for 4h 48 min with a ×60 objective, in which an additional zoom of ×2.18 was achieved. We also used the multiposition setting to increase the chance of visualizing bacterial killing activity and ZDC control to keep the sample in focus during the length of the time-lapse video and prevent focal drift. In total, eight time-lapse videos have been produced for each competition assay ($n = 8$ videos with *Xt* UPB513 WT; $n = 8$ videos with *Xt* UPB513 ΔT6SS-i4; from several positions on the same sample each).

Comparative genetic and phylogenetic analyses

The matrix of average nucleotide identity (AVI) was calculated using Pyani 0.2.11 (ref. 62) (Supplementary Fig. 9) with the option -ANIm, and the ANI-Matrix software Enveomics tool[63]. Visualization of groups of homologous gene clusters was performed using Clinker v.0.0.27 (ref. 64). To study the evolutionary history of X-T4SS and T6SS-i4, the amino acid sequences of the VirD4 and TssC proteins were extracted for each type strain of selected *Xanthomonas* species. MEGA11 was used for amino acid sequence alignment with ClustalW followed by IQ-TREE web server (http://iqtree.cibiv.univie.ac.at/) for inferring phylogenetic tree using maximum likelihood with default parameters[60,65]. The species phylogenetic tree was then inferred using kSNP3 using *k*-mer of 21 bp (X-T4SS) and 23 bp (T6SS-i4). The VirB8 phylogenetic tree was constructed with the automated multilocus sequence analysis pipeline (autoMLSA2) 0.8.1 (ref. 66) using the VirB8 amino acid sequence from *X. citri* 306 as a query. iTOL (https://itol.embl.de/) was then used to display and annotate phylogenetic trees[67]. X-T4SS and T6SS-i4 neighbourhoods were determined using Benchling and Clinker and manually checked in detail. GIs were detected using IslandViewer4 (https://www.pathogenomics.sfu.ca/islandviewer/)[29].

Comparison of X-T4SS and T6SS-i4 effector arsenals. To compare the effector arsenals of X-T4SS and T6SS-i4, we analysed pairs of genetically close *Xanthomonas* strains carrying either system. We selected three pairs of *Xt* (clade 1) and one pair of *Xanthomonas vesicatoria* (*Xv*; clade 2): *Xt* pv. *phlei/phleipratensis* LMG 843 and LMG 730; *Xt* pv. *translucens* UPB886 and DSM 18974; *Xt* pv. *graminis* NCPPB 3709 and NCPPB 3711; and *Xv* BNM214 and LMG 911. To identify X-T4SS effectors, the HMM profile of the C-terminal XVIPCD translocation domain was retrieved from Pfam. For T6SS effectors, different HMM profiles of domains frequently found in T6SS effectors were selected: MIX, FIX, VgrG, PAAR, Rhs and so on, also retrieved from Pfam (Supplementary Table 3). HMM search were conducted against the predicted proteome, as annotated in the NCBI RefSeq files, of each strain. Genes found downstream of a VgrG/Hcp/PAAR-containing protein were further analysed to detect candidate toxic effectors in the vicinity. The resulting candidate effectors were analysed by InterProScan to predict protein domains[68] (Supplementary Tables 1–3). They were then manually analysed to check for pseudogenes, due to frameshifts, early in-frame stop codons or IS elements.

Reporting summary

Further information on research design is available in the Nature Portfolio Reporting Summary linked to this article.

Data availability

All data supporting the findings of this study are available in the paper and Supplementary Information and as source data files via Zenodo at https://doi.org/10.5281/zenodo.15367606 (ref. 69). Further information and requests for resources and reagents should be directed to C.B. (claude.bragard@uclouvain.be). Bacterial strains and plasmids used in this study can be made available on request following the signing of a material transfer agreement.

Code availability

Code for the data statistical analyses is available via Zenodo at https://doi.org/10.5281/zenodo.15367606 (ref. 69).

References

1. Granato, E. T., Meiller-Legrand, T. A. & Foster, K. R. The evolution and ecology of bacterial warfare. *Curr. Biol.* **29**, R521–R537 (2019).
2. Booth, S. C., Smith, W. P. J. & Foster, K. R. The evolution of short- and long-range weapons for bacterial competition. *Nat. Ecol. Evol.* **7**, 2080–2091 (2023).
3. Jacques, M. A. et al. Using ecology, physiology, and genomics to understand host specificity in *Xanthomonas*. *Annu. Rev. Phytopathol.* **54**, 163–187 (2016).
4. An, S. Q. et al. Mechanistic insights into host adaptation, virulence and epidemiology of the phytopathogen *Xanthomonas*. *FEMS Microbiol. Rev.* **44**, 1–32 (2020).
5. Souza, D. P. et al. Bacterial killing via a type IV secretion system. *Nat. Commun.* **6**, 6453 (2015).
6. Zhu, P. C. et al. Type VI secretion system is not required for virulence on rice but for inter-bacterial competition in *Xanthomonas oryzae* pv. *oryzicola*. *Res. Microbiol.* **171**, 64–73 (2020).

7. Bayer-Santos, E., DeMoraes Ceseti, L., Farah, C. S. & Alvarez-Martinez, C. E. Distribution, function and regulation of type 6 secretion systems of Xanthomonadales. *Front. Microbiol.* **10**, 1635 (2019).
8. Sgro, G. G. et al. Bacteria-killing type IV secretion systems. *Front. Microbiol.* **10**, 1078 (2019).
9. Boyer, F., Fichant, G., Berthod, J., Vandenbrouck, Y. & Attree, I. Dissecting the bacterial type VI secretion system by a genome wide in silico analysis: what can be learned from available microbial genomic resources? *BMC Genomics* **10**, 104 (2009).
10. Bernal, P., Llamas, M. A. & Filloux, A. Type VI secretion systems in plant-associated bacteria. *Environ. Microbiol.* **20**, 1–15 (2018).
11. Gallique, M., Bouteiller, M. & Merieau, A. The type VI secretion system: a dynamic system for bacterial communication? *Front. Microbiol.* **8**, 1454 (2017).
12. Costa, T. R. D. et al. Secretion systems in Gram-negative bacteria: structural and mechanistic insights. *Nat. Rev. Microbiol.* **13**, 343–359 (2015).
13. Allsopp, L. P. & Bernal, P. Killing in the name of: T6SS structure and effector diversity. *Microbiology* **169**, 001367 (2023).
14. Alvarez-Martinez, C. E. et al. Secrete or perish: the role of secretion systems in *Xanthomonas* biology. *Comput. Struct. Biotechnol. J.* **19**, 279–302 (2020).
15. Sgro, G. G. et al. Cryo-EM structure of the bacteria-killing type IV secretion system core complex from *Xanthomonas citri*. *Nat. Microbiol.* **3**, 1429–1440 (2018).
16. Souza, D. P. et al. A component of the Xanthomonadaceae type IV secretion system combines a VirB7 motif with a N0 domain found in outer membrane transport proteins. *PLoS Pathog.* **7**, e1002031 (2011).
17. Bragard, C. et al. *Xanthomonas translucens* from small grains: diversity and phytopathological relevance. *Phytopathology* **87**, 1111–1117 (1997).
18. Goettelmann, F. et al. Complete genome assemblies of all *Xanthomonas translucens* pathotype strains reveal three genetically distinct clades. *Front. Microbiol.* **12**, 817815 (2022).
19. Bi, D. et al. SecReT4: a web-based bacterial type IV secretion system resource. *Nucleic Acids Res.* **41**, D660–D665 (2013).
20. Zhang, J. et al. SecReT6 update: a comprehensive resource of bacterial Type VI secretion systems. *Sci. China Life Sci.* **66**, 626–634 (2023).
21. Altschul, S. F., Gish, W., Miller, W., Myers, E. W. & Lipman, D. J. Basic local alignment search tool. *J. Mol. Biol.* **215**, 403–410 (1990).
22. Heiden, N., Roman-Reyna, V., Curland, R. D., Dill-Macky, R. & Jacobs, J. M. Comparative genomics of Minnesotan barley-infecting *Xanthomonas translucens* shows overall genomic similarity but virulence factor diversity. *Phytopathology* **113**, 2056–2061 (2023).
23. Durfee, T. et al. The complete genome sequence of *Escherichia coli* DH10B: insights into the biology of a laboratory workhorse. *J. Bacteriol.* **190**, 2597–2606 (2008).
24. Dubois, B. et al. PRONAME: a user-friendly pipeline to process long-read nanopore metabarcoding data by generating high-quality consensus sequences. *Front. Bioinform.* **4**, 1483255 (2024).
25. Bayer-Santos, E. et al. The opportunistic pathogen *Stenotrophomonas maltophilia* utilizes a type IV secretion system for interbacterial killing. *PLoS Pathog.* **15**, e1007651 (2019).
26. Campos, P. E. et al. Herbarium specimen sequencing allows precise dating of *Xanthomonas citri* pv. *citri* diversification history. *Nat. Commun.* **14**, 4306 (2023).
27. Speare, L. et al. Bacterial symbionts use a type VI secretion system to eliminate competitors in their natural host. *Proc. Natl Acad. Sci. USA* **115**, E8528–E8537 (2018).
28. Dobrindt, U., Hochhut, B., Hentschel, U. & Hacker, J. Genomic islands in pathogenic and environmental microorganisms. *Nat. Rev. Microbiol.* **2**, 414–424 (2004).
29. Bertelli, C. et al. IslandViewer 4: expanded prediction of genomic islands for larger-scale datasets. *Nucleic Acids Res.* **45**, W30–W35 (2017).
30. Shao, Y. et al. Transcriptional regulator Sar regulates the multiple secretion systems in *Xanthomonas oryzae*. *Mol. Plant Pathol.* **24**, 16–27 (2023).
31. Garin, T. et al. The type VI secretion system of *Stenotrophomonas rhizophila* CFBP13503 limits the transmission of *Xanthomonas campestris* pv. *campestris* 8004 from radish seeds to seedlings. *Mol. Plant Pathol.* **25**, e13412 (2024).
32. Shen, X. et al. *Lysobacter enzymogenes* antagonizes soilborne bacteria using the type IV secretion system. *Environ. Microbiol.* **23**, 4673–4688 (2021).
33. Yu, M., Zhang, G., Jiang, J., Du, L. & Zhao, Y. *Lysobacter enzymogenes* employs diverse genes for inhibiting hypha growth and spore germination of soybean fungal pathogens. *Phytopathology* **110**, 593–602 (2020).
34. Fronzes, R., Christie, P. J. & Waksman, G. The structural biology of type IV secretion systems. *Nat. Rev. Microbiol.* **7**, 703–714 (2009).
35. Soufiane, B., Sirois, M. & Côté, J. C. Mutually exclusive distribution of the sap and eag S-layer genes and the lytB/lytA cell wall hydrolase genes in *Bacillus thuringiensis*. *Antonie Van Leeuwenhoek* **100**, 349–364 (2011).
36. Rossi, P. et al. Mutual exclusion of Asaia and Wolbachia in the reproductive organs of mosquito vectors. *Parasit. Vectors* **8**, 278 (2015).
37. Zhang, X., Kupiec, M., Gophna, U. & Tuller, T. Analysis of coevolving gene families using mutually exclusive orthologous modules. *Genome Biol. Evol.* **3**, 413–423 (2011).
38. Cenens, W. et al. Bactericidal type IV secretion system homeostasis in *Xanthomonas citri*. *PLoS Pathog.* **16**, e1008561 (2020).
39. Che, S. et al. T6SS and T4SS redundantly secrete effectors to govern the virulence and bacterial competition in pectobacterium PccS1. *Phytopathology* **114**, 1926–1939 (2024).
40. Liyanapathiranage, P., Wagner, N., Avram, O., Pupko, T. & Potnis, N. Phylogenetic distribution and evolution of type VI secretion system in the genus *Xanthomonas*. *Front. Microbiol.* **13**, 840308 (2022).
41. Kirchberger, P. C., Unterweger, D., Provenzano, D., Pukatzki, S. & Boucher, Y. Sequential displacement of type VI secretion system effector genes leads to evolution of diverse immunity gene arrays in *Vibrio cholerae*. *Sci. Rep.* **7**, 45133 (2017).
42. Taillefer, B., Giraud, J. F. & Cascales, E. No fitness cost entailed by type VI secretion system synthesis, assembly, contraction, or disassembly in enteroaggregative *Escherichia coli*. *J. Bacteriol.* **205**, e0035723 (2023).
43. Zhang, C., Datta, S., Ratcliff, W. C. & Hammer, B. K. Constitutive expression of the type VI secretion system carries no measurable fitness cost in *Vibrio cholerae*. *Ecol. Evol.* **14**, e11081 (2024).
44. Robitaille, S. et al. Community composition and the environment modulate the population dynamics of type VI secretion in human gut bacteria. *Nat. Ecol. Evol.* **7**, 2092–2107 (2023).
45. Unni, R., Pintor, K. L., Diepold, A. & Unterweger, D. Presence and absence of type VI secretion systems in bacteria. *Microbiology* **168**, 001151 (2022).
46. Gluck-Thaler, E. et al. Repeated gain and loss of a single gene modulates the evolution of vascular plant pathogen lifestyles. *Sci. Adv.* **6**, eabc4516 (2020).
47. Cesbron, S. et al. Comparative genomics of pathogenic and nonpathogenic strains of *Xanthomonas arboricola* unveil molecular and evolutionary events linked to pathoadaptation. *Front. Plant Sci.* **6**, 1126 (2015).

48. de Assis, J. C. S. et al. Genomic analysis reveals the role of integrative and conjugative elements in plant pathogenic bacteria. *Mob. DNA* **13**, 19 (2022).
49. Juhas, M., Crook, D. W. & Hood, D. W. Type IV secretion systems: tools of bacterial horizontal gene transfer and virulence. *Cell Microbiol.* **10**, 2377–2386 (2008).
50. Peñil-Celis, A. & Garcillán-Barcia, M. P. Crosstalk between type VI secretion system and mobile genetic elements. *Front. Mol. Biosci.* **6**, 126 (2019).
51. Morgado, S. & Vicente, A. C. Diversity and distribution of type VI secretion system gene clusters in bacterial plasmids. *Sci. Rep.* **12**, 8249 (2022).
52. García-Bayona, L., Coyne, M. J. & Comstock, L. E. Mobile type VI secretion system loci of the gut Bacteroidales display extensive intra-ecosystem transfer, multi-species spread and geographical clustering. *PLoS Genet.* **17**, e1009541 (2021).
53. Bayer-Santos, E. et al. *Xanthomonas citri* T6SS mediates resistance to *Dictyostelium* predation and is regulated by an ECF σ factor and cognate Ser/Thr kinase. *Environ. Microbiol.* **20**, 1562–1575 (2018).
54. Choi, Y. et al. Characterization of type VI secretion system in *Xanthomonas oryzae* pv. *oryzae* and its role in virulence to rice. *Plant Pathol. J.* **36**, 289–296 (2020).
55. Schäfer, A. et al. Small mobilizable multi-purpose cloning vectors derived from the *Escherichia coli* plasmids pK18 and pK19: selection of defined deletions in the chromosome of *Corynebacterium glutamicum*. *Gene* **145**, 69–73 (1994).
56. Choi, K. H. & Schweizer, H. P. mini-Tn7 insertion in bacteria with single attTn7 sites: example *Pseudomonas aeruginosa*. *Nat. Protoc.* **1**, 153–161 (2006).
57. Hadfield, J. D. MCMC methods for multi-response generalized linear mixed models: the MCMCglmm R package. *J. Stat. Softw.* https://doi.org/10.18637/jss.v033.i02 (2010).
58. Jain, C., Rodriguez-R, L. M., Phillippy, A. M., Konstantinidis, K. T. & Aluru, S. High throughput ANI analysis of 90K prokaryotic genomes reveals clear species boundaries. *Nat. Commun.* **9**, 5114 (2018).
59. Jalili, V. et al. The Galaxy platform for accessible, reproducible and collaborative biomedical analyses: 2020 update. *Nucleic Acids Res.* **48**, W395–W402 (2021).
60. Tamura, K., Stecher, G. & Kumar, S. MEGA11: molecular evolutionary genetics analysis version 11. *Mol. Biol. Evol.* **38**, 3022–3027 (2021).
61. Sokal, R. & Michener, C. A statistical method for evaluating systematic relationships. *Univ. Kans. Sci. Bull.* **38**, 1409–1438 (1958).
62. Pritchard, L. et al. Pyani: whole-genome classification using average nucleotide identity. *Zenodo* https://doi.org/10.5281/ZENODO.594921 (2015).
63. Rodriguez-R, L. M. & Konstantinidis, K. T. The enveomics collection: a toolbox for specialized analyses of microbial genomes and metagenomes. *PeerJ Preprints* **4**, e1900v1 (2016).
64. Gilchrist, C. L. M. & Chooi, Y. H. clinker & clustermap.js: automatic generation of gene cluster comparison figures. *Bioinformatics* **37**, 2473–2475 (2021).
65. Trifinopoulos, J., Nguyen, L. T., von Haeseler, A. & Minh, B. Q. W-IQ-TREE: a fast online phylogenetic tool for maximum likelihood analysis. *Nucleic Acids Res.* **44**, W232–W235 (2016).
66. Davis, E. W., Okrent, R. A., Manning, V. A. & Trippe, K. M. Unexpected distribution of the 4-formylaminooxyvinylglycine (FVG) biosynthetic pathway in *Pseudomonas* and beyond. *PLoS ONE* **16**, e0247348 (2021).
67. Letunic, I. & Bork, P. Interactive Tree of Life (iTOL) v6: recent updates to the phylogenetic tree display and annotation tool. *Nucleic Acids Res.* **52**, W78–W82 (2024).
68. Jones, P. et al. InterProScan 5: genome-scale protein function classification. *Bioinformatics* **30**, 1236–1240 (2014).
69. Peduzzi, C. & Bragard, C. Functional replacement of ancestral antibacterial secretion system in a bacterial plant pathogen. *Zenodo* https://doi.org/10.5281/zenodo.15367606 (2025).

Acknowledgements

We thank The Ohio Supercomputer Center for providing high-performance computing resources and microscope and imaging specialist D. Ignacio from Hunt Optics and Imaging Inc. Olympus for his valuable help in designing and optimizing laser scanning confocal microscope parameters for time-lapse videos. We would like to thank J. Mahillon (UCLouvain, Louvain-la-Neuve, Belgium) for his precious advice and for enriching intellectual discussions and L. M. Rodriguez-R (University of Innsbruck, Austria) for fruitful discussions. C.P. was supported by the Foundation for Training in Industrial and Agricultural Research (FRIA, FNRS) (grant no. 40021596). Part of this article is based on work from COST Action CA16107 EuroXanth, supported by COST (European Cooperation in Science and Technology) (C.P., R.K. and C.B.). We are grateful for support from a Fulbright Scholar Award to Uruguay to J.M.J.

Author contributions

C.P., C.B., R.K. and J.M.J. designed the study and C.B., R.K. and J.M.J. supervised the conducted research. C.P., J.B. and F.N. performed the experiments. C.P. performed bioinformatic analyses. C.P. and M.M. performed statistical analyses. J.B., N.H. and M.V.M. assisted with the experiments and V.R.-R. and R.K. assisted with the bioinformatic analyses. C.P. wrote the manuscript and all authors discussed the results and edited the manuscript.

Competing interests

The authors declare no competing interests.

Additional information

Extended data is available for this paper at https://doi.org/10.1038/s41559-025-02773-w.

Supplementary information The online version contains supplementary material available at https://doi.org/10.1038/s41559-025-02773-w.

Correspondence and requests for materials should be addressed to Claude Bragard.

Peer review information *Nature Ecology & Evolution* thanks William Smith and the other, anonymous, reviewer(s) for their contribution to the peer review of this work. Peer reviewer reports are available.

https://doi.org/10.1038/s41559-025-02773-w

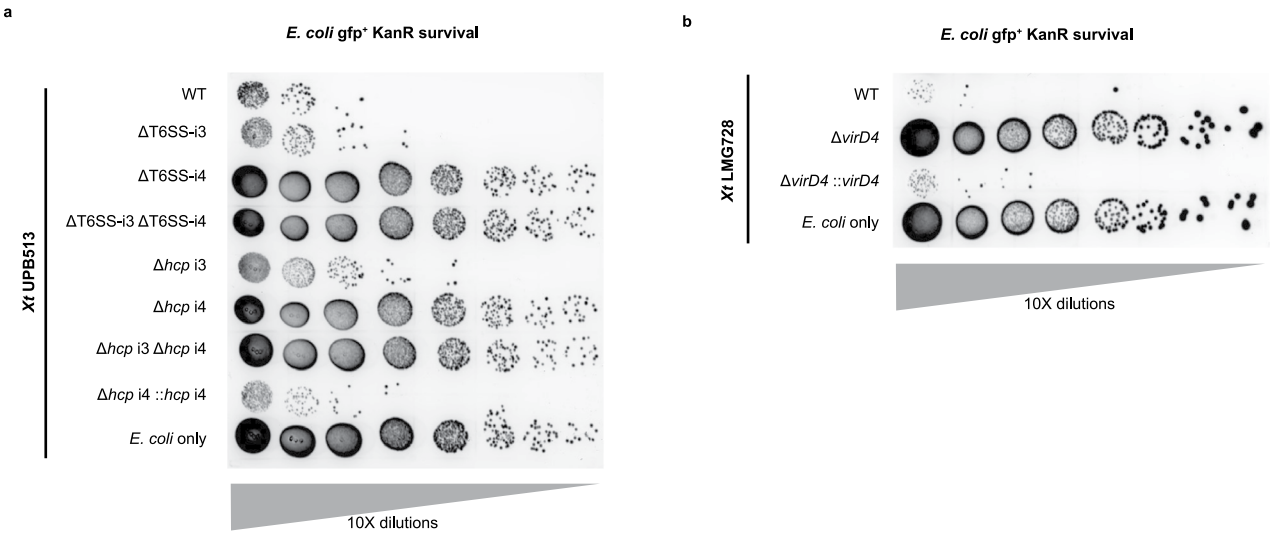

Extended Data Fig. 1 | *Xt* (a) T6SS-i4 and (b) X-T4SS are required for inter-bacterial competition. Representative NA plates with tenfold dilution series of the quantitative assay showing *E. coli* survival using Amersham Typhoon laser scanner.

https://doi.org/10.1038/s41559-025-02773-w

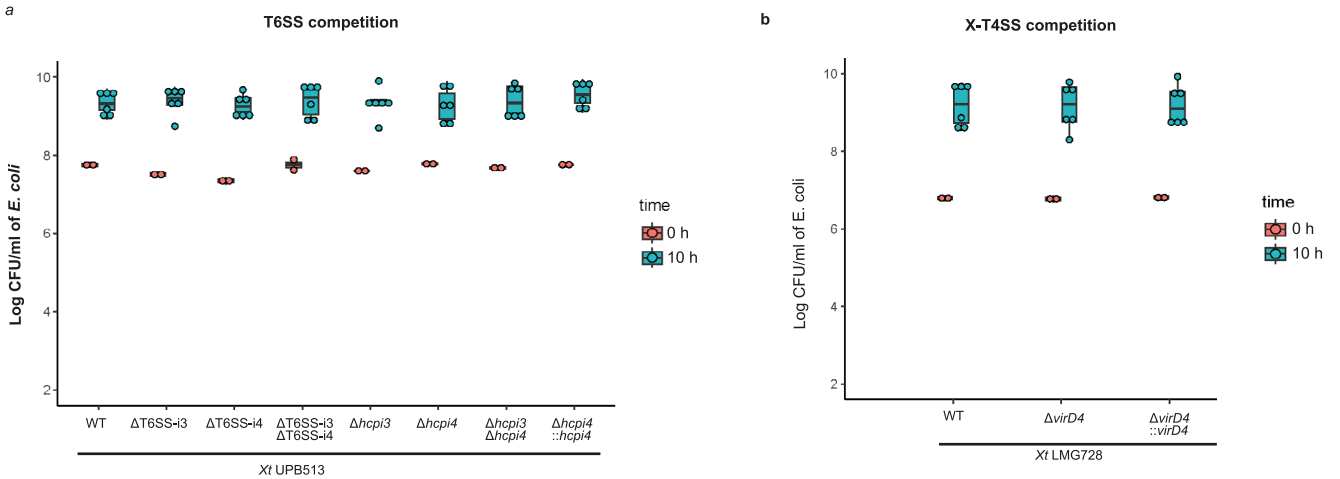

Extended Data Fig. 2 | *Xt* growth is not impacted by (a) T6SS and (b) X-T4SS mutations during bacterial competition assays against *E. coli*. Quantitative competition assay with *E. coli* mixed in a 10:1 ratio (*Xt*:*E. coli*) for 10 h of co-cultivation. Boxplot represents *Xt* growth log CFU/ml after 0 h and 10 h of co-cultivation. All boxplots show 1st and 3rd quartiles around the median. Whiskers represent the smallest and largest value no further than 1.5 * IQR (inter-quartile range) from the hinge. Dots indicate independent biological replicates (n = 2 at 0 h; n = 6 at 10 h). Significance was tested by two-sided Student's T-test. Significance codes: *** ($P < 0.001$), ** ($P < 0.01$), * ($P < 0.05$), only significant comparisons are shown (ΔT6SS-i3: $P = 1$, ΔT6SS-i4: $P = 1$, ΔT6SS-i3 ΔT6SS-i4: $P = 1$, Δ*hcpi3*: $P = 1$, Δ*hcpi4*: $P = 1$, Δ*hcpi3* Δ*hcpi4*: $P = 1$, and Δ*hcpi4*::*hcpi4*: $P = 1$; Δ*virD4*: $P = 1$, and Δ*virD4*::*virD4*: $P = 1$).

https://doi.org/10.1038/s41559-025-02773-w

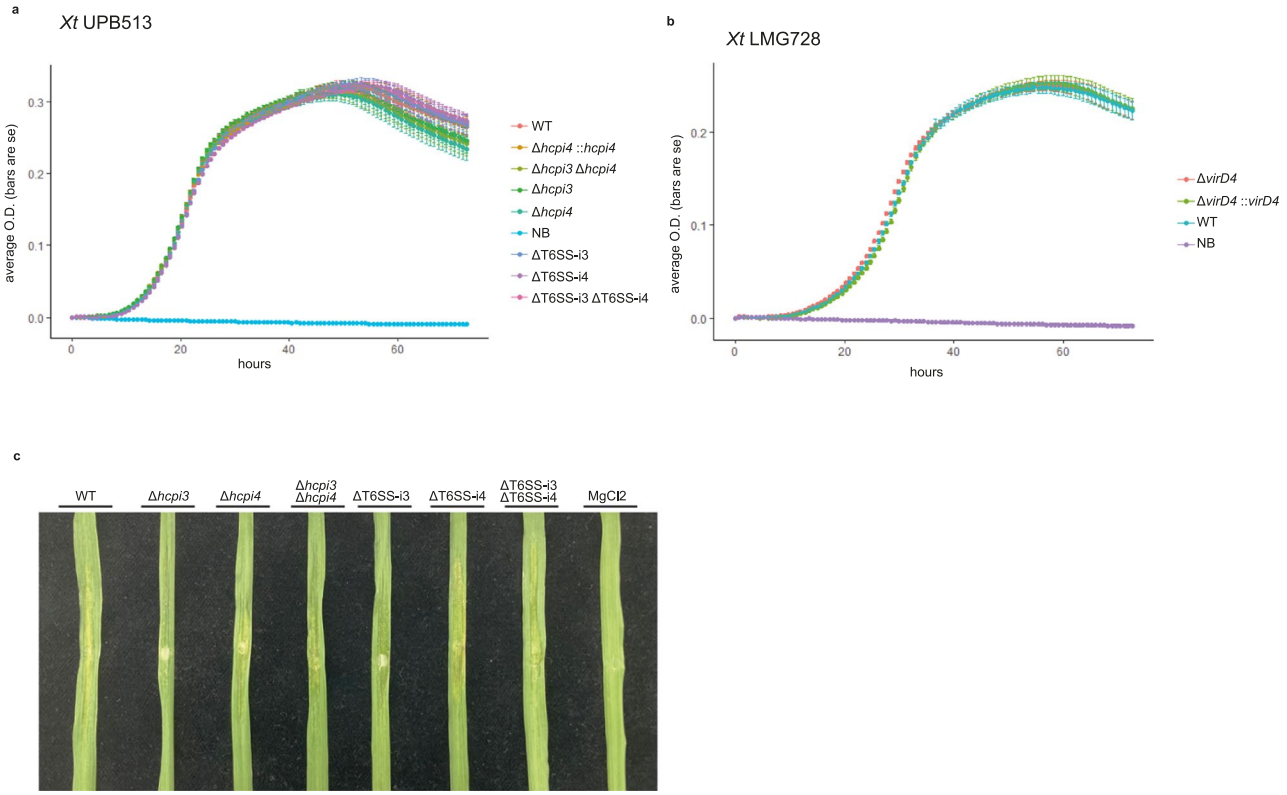

Extended Data Fig. 3 | Phenotypic characterization of *Xt* UPB513 T6SS and X-T4SS mutants. (a, b) *In vitro* growth curve of **(a)** *Xt* UPB513 WT and derived strains mutated in and complemented for T6SS, **(b)** *Xt* LMG728 WT and derived strains mutants in and complemented for T4SS, in NB medium at 28 °C, OD_{600} measured at 45-minute intervals. Dots represent mean and error bars show s.e.m (n = 8 replicates per strain). **(c)** Barley cv. Hercule leaves infiltrated with *Xtu* UPB513 WT or T6SS mutants show water-soaking and necrotic lesions at 6 dpi (n = 8 plants).

https://doi.org/10.1038/s41559-025-02773-w

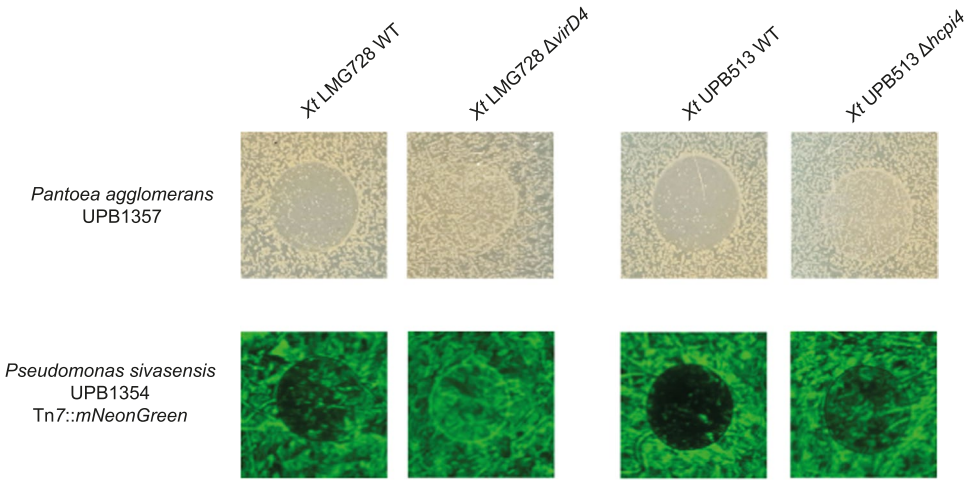

Extended Data Fig. 4 | *Xt* T6SS-i4 and X-T4SS are required for inter-bacterial competition against *Pseudomonas* sp. and *Pantoea* sp. Representative qualitative competition plate using *Xt* UPB513 WT, Δ*hcpi4*, *Xt* LMG728 WT and Δ*virD4* as attacker cells and *Pantoea agglomerans* UPB1357 and *Pseudomonas sivasensis* UPB1354 Tn*7*::*mNeonGreen* as target cells after 16 h of competition on NA.

https://doi.org/10.1038/s41559-025-02773-w

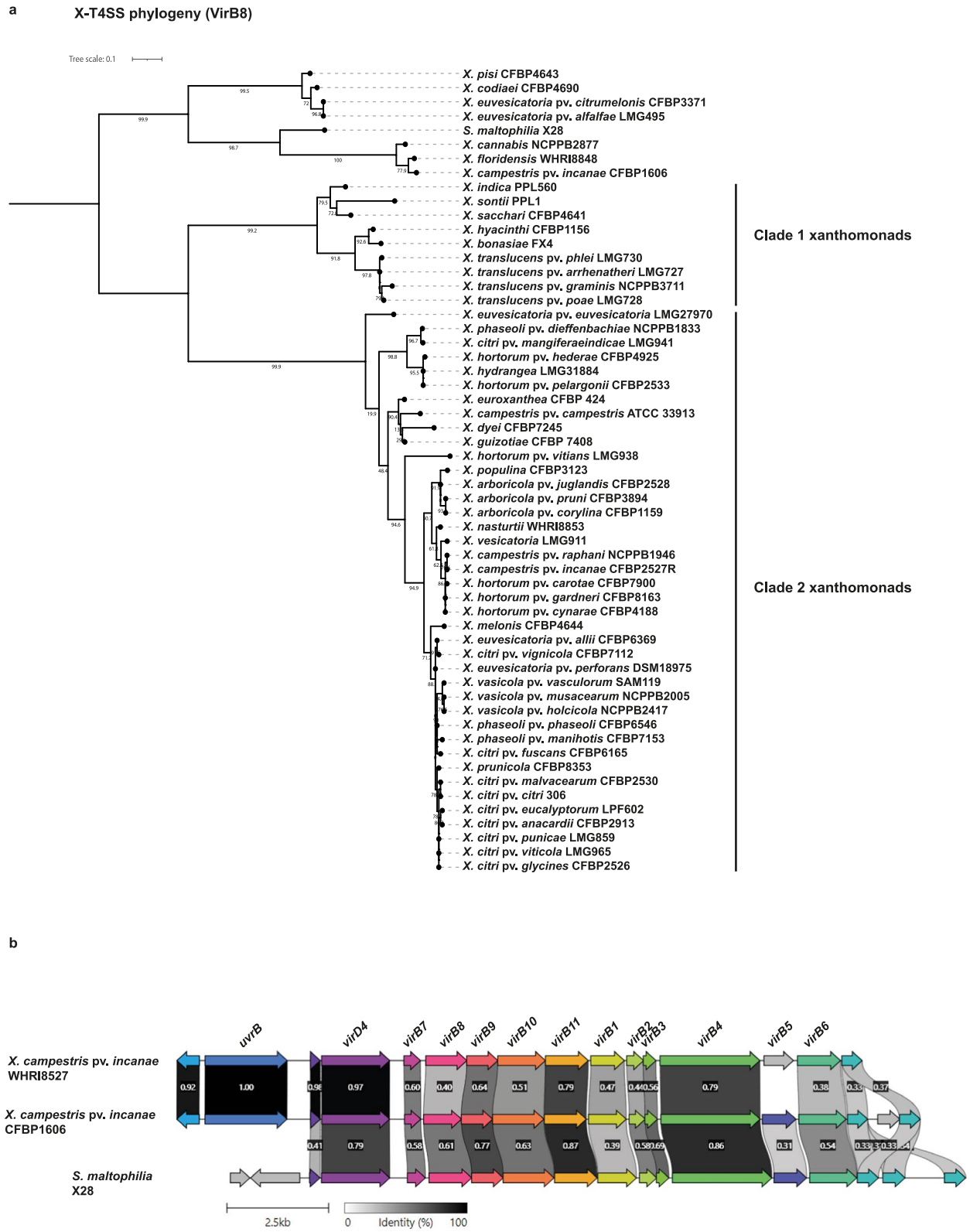

Extended Data Fig. 5 | VirB8-based phylogeny reveals xanthomonads with atypical X-T4SS sequences. (a) The phylogenetic tree was constructed using autoMLSA2, by extracting and aligning VirB8 amino acid sequences from each type/pathotype strain of each *Xanthomonas* species and pathovar possessing X-T4SS and using IQ-TREE to infer the phylogenetic tree. **(b)** Comparison of the T4SS gene clusters from *X. campestris* pv. *incanae* and *Stenotrophomonas maltophilia*. Most X-T4SS genes (except for *virD4*) of strain CFBP 1606 share higher sequence identity with the corresponding genes from strain X28 than with those in strain WHRI 8527.

https://doi.org/10.1038/s41559-025-02773-w

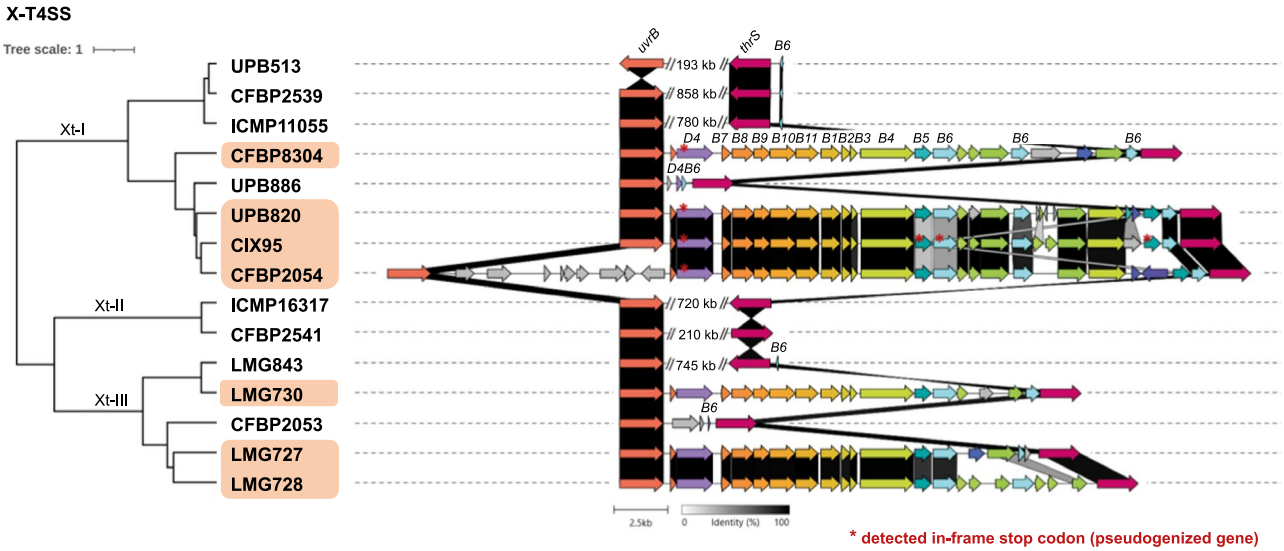

Extended Data Fig. 6 | Various decay and loss events occurred in the X-T4SS clusters. The tree on the left side is based on average nucleotide identity (ANI) of *Xt* strains, whereas the right side provides an overview of the organization of the X-T4SS gene clusters and their neighboring genes *uvrB* and *thrS*. Letters and numbers above the genes correspond to the *virD* and *virB* genes. Scales for distance and percentage identity between genes are indicated below. Genes are color-coded according to homology. Pseudogenized genes are highlighted with an asterisk. Fragments of remnant X-T4SS genes are found within the corresponding genomic location in the X-T4SS-lacking strains. The three ANI clades Xt-I, Xt-II and Xt-III are indicated in the tree.

https://doi.org/10.1038/s41559-025-02773-w

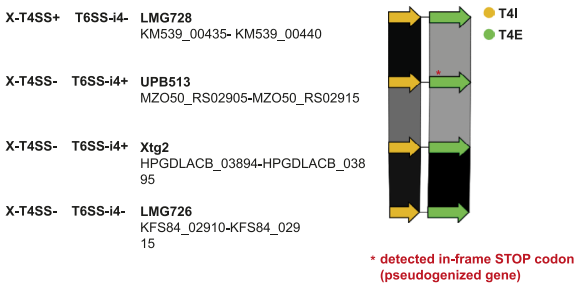

Extended Data Fig. 7 | X-T4SS-lacking strains possess T4E-T4I pairs. Comparison of candidate X-T4SS effector-immunity pairs across strains possessing either X-T4SS, T6SS-i4, or none of them. The asterisk indicates an in-frame STOP codon.

https://doi.org/10.1038/s41559-025-02773-w

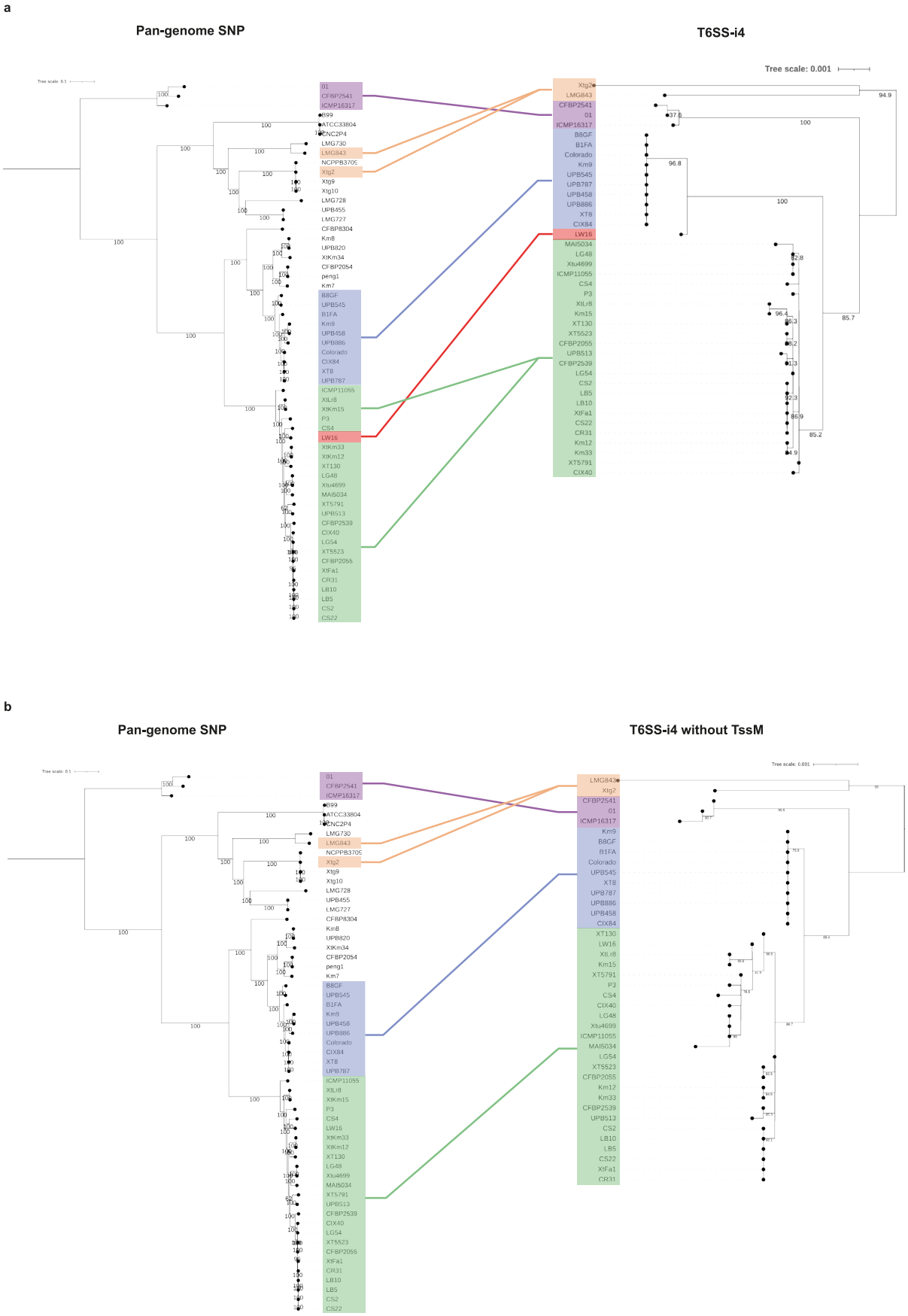

Extended Data Fig. 8 | See next page for caption.

https://doi.org/10.1038/s41559-025-02773-w

Extended Data Fig. 8 | Incongruency between the T6SS-i4 and the pan-genome tree topology of strain *Xt* LW16 is caused by the *tssM* gene. Comparison between species (left) and T6SS-i4 (right) phylogenies. The pan-genome SNP-based tree was constructed using kSNP3 (kmer of 23 bp). The T6SS-i4 tree was inferred by maximum likelihood using IQ-TREE based on concatenated alignment of *tssA, tssB, tssC, tssD, tssE, tssF, tssG, tssH, tssK, tssL* , **(a)** with or **(b)** without *tssM* genes. Amino acid sequences were aligned by ClustalW. The bootstrap supports were estimated based on 1000 replicates. Trees were visualized with iTOL.

https://doi.org/10.1038/s41559-025-02773-w

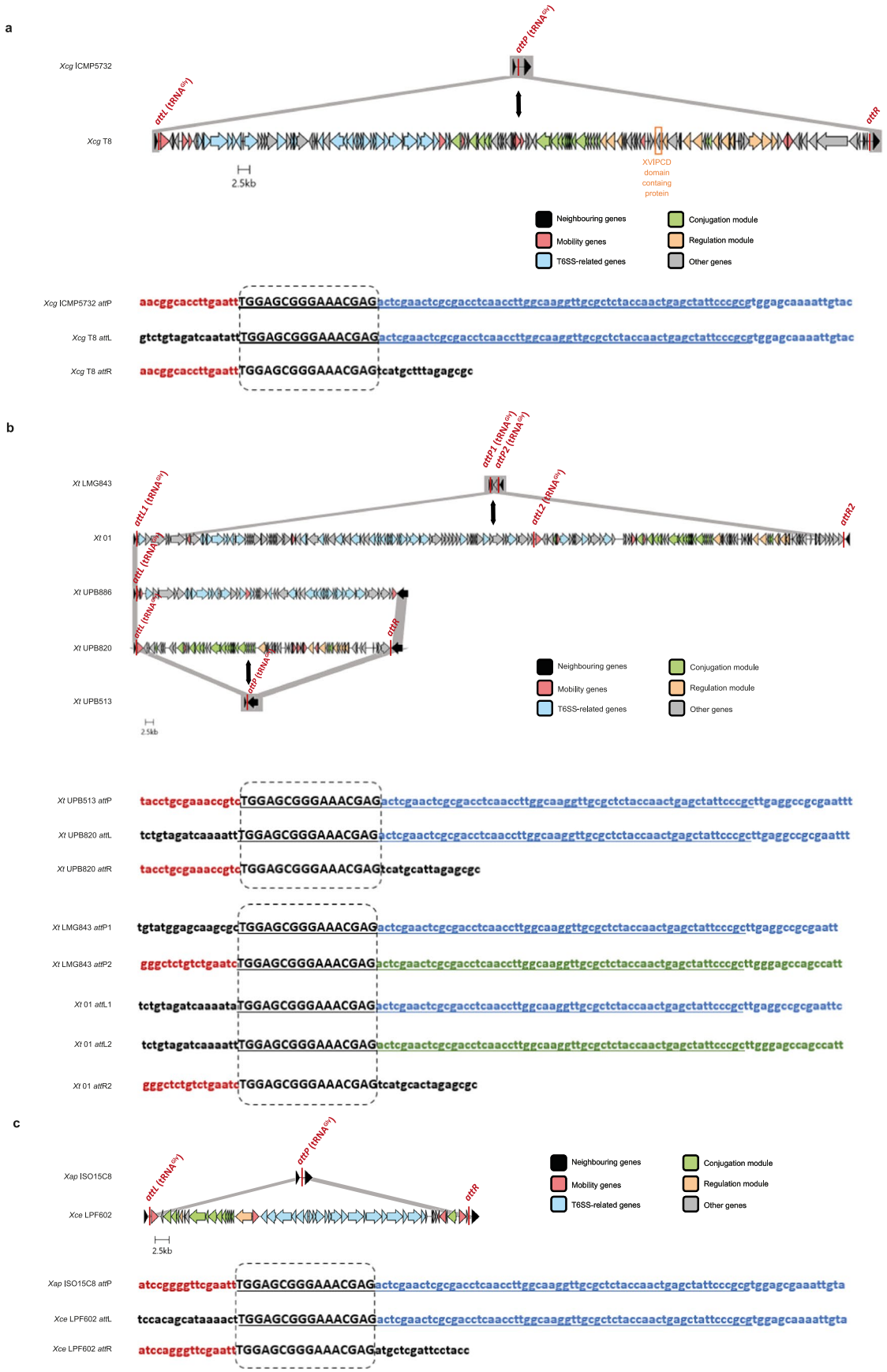

Extended Data Fig. 9 | T6SS-i4 and ICE in type-2 neighborhood are flanked by *att* sites in strains (a) *Xcg* T8, (b) *Xt* 01, *Xt* UPB886, *Xt* UPB820 and (c) *Xce* LPF602. (Upper panel) Genes corresponding to the same ICE modules are represented in similar colors. Genes with unknown functions are indicated in gray. *attL* and *attR* sites flanking the GI and *attP* in the T6SS-i4 lacking strain are pointed with red bars. (Lower panel) *attL*, *attR* and *attP* sites sequences are shown, 16-bp direct repeat sequences are boxed with dashed lines and tRNA-Gly sequences are underlined.

nature portfolio

Corresponding author(s): claude.bragard@uclouvain.be

Last updated by author(s): May 9, 2025

Reporting Summary

Nature Portfolio wishes to improve the reproducibility of the work that we publish. This form provides structure for consistency and transparency in reporting. For further information on Nature Portfolio policies, see our Editorial Policies and the Editorial Policy Checklist.

Statistics

For all statistical analyses, confirm that the following items are present in the figure legend, table legend, main text, or Methods section.

n/a	Confirmed	
☐	☒	The exact sample size (*n*) for each experimental group/condition, given as a discrete number and unit of measurement
☐	☒	A statement on whether measurements were taken from distinct samples or whether the same sample was measured repeatedly
☐	☒	The statistical test(s) used AND whether they are one- or two-sided *Only common tests should be described solely by name; describe more complex techniques in the Methods section.*
☐	☒	A description of all covariates tested
☐	☒	A description of any assumptions or corrections, such as tests of normality and adjustment for multiple comparisons
☐	☒	A full description of the statistical parameters including central tendency (e.g. means) or other basic estimates (e.g. regression coefficient) AND variation (e.g. standard deviation) or associated estimates of uncertainty (e.g. confidence intervals)
☐	☒	For null hypothesis testing, the test statistic (e.g. *F*, *t*, *r*) with confidence intervals, effect sizes, degrees of freedom and *P* value noted *Give P values as exact values whenever suitable.*
☐	☒	For Bayesian analysis, information on the choice of priors and Markov chain Monte Carlo settings
☒	☐	For hierarchical and complex designs, identification of the appropriate level for tests and full reporting of outcomes
☒	☐	Estimates of effect sizes (e.g. Cohen's *d*, Pearson's *r*), indicating how they were calculated

Our web collection on statistics for biologists contains articles on many of the points above.

Software and code

Policy information about availability of computer code

Data collection	No custom algorithms or software was used.
Data analysis	Description of all commercial, open source code and versions used to analyse the data has been made available in the section method.

For manuscripts utilizing custom algorithms or software that are central to the research but not yet described in published literature, software must be made available to editors and reviewers. We strongly encourage code deposition in a community repository (e.g. GitHub). See the Nature Portfolio guidelines for submitting code & software for further information.

Data

Policy information about availability of data

All manuscripts must include a data availability statement. This statement should provide the following information, where applicable:

- Accession codes, unique identifiers, or web links for publicly available datasets
- A description of any restrictions on data availability
- For clinical datasets or third party data, please ensure that the statement adheres to our policy

All data supporting the findings of this study are available within the paper, its Supplementary Information and as Source Data files on Zenodo at the following DOI: https://zenodo.org/records/15367606. Further information and requests for resources and reagents should be directed to Claude Bragard (claude.bragard@uclouvain.be). Bacterial strains and plasmids used in this study can be made available upon request following the signing of a material transfer agreement

Genome data of this study are being made directly available.

Research involving human participants, their data, or biological material

Policy information about studies with human participants or human data. See also policy information about sex, gender (identity/presentation), and sexual orientation and race, ethnicity and racism.

Reporting on sex and gender	*Use the terms sex (biological attribute) and gender (shaped by social and cultural circumstances) carefully in order to avoid confusing both terms. Indicate if findings apply to only one sex or gender; describe whether sex and gender were considered in study design; whether sex and/or gender was determined based on self-reporting or assigned and methods used.* *Provide in the source data disaggregated sex and gender data, where this information has been collected, and if consent has been obtained for sharing of individual-level data; provide overall numbers in this Reporting Summary. Please state if this information has not been collected.* *Report sex- and gender-based analyses where performed, justify reasons for lack of sex- and gender-based analysis.*
Reporting on race, ethnicity, or other socially relevant groupings	*Please specify the socially constructed or socially relevant categorization variable(s) used in your manuscript and explain why they were used. Please note that such variables should not be used as proxies for other socially constructed/relevant variables (for example, race or ethnicity should not be used as a proxy for socioeconomic status).* *Provide clear definitions of the relevant terms used, how they were provided (by the participants/respondents, the researchers, or third parties), and the method(s) used to classify people into the different categories (e.g. self-report, census or administrative data, social media data, etc.)* *Please provide details about how you controlled for confounding variables in your analyses.*
Population characteristics	*Describe the covariate-relevant population characteristics of the human research participants (e.g. age, genotypic information, past and current diagnosis and treatment categories). If you filled out the behavioural & social sciences study design questions and have nothing to add here, write "See above."*
Recruitment	*Describe how participants were recruited. Outline any potential self-selection bias or other biases that may be present and how these are likely to impact results.*
Ethics oversight	*Identify the organization(s) that approved the study protocol.*

Note that full information on the approval of the study protocol must also be provided in the manuscript.

Field-specific reporting

Please select the one below that is the best fit for your research. If you are not sure, read the appropriate sections before making your selection.

☒ Life sciences ☐ Behavioural & social sciences ☐ Ecological, evolutionary & environmental sciences

For a reference copy of the document with all sections, see nature.com/documents/nr-reporting-summary-flat.pdf

Life sciences study design

All studies must disclose on these points even when the disclosure is negative.

Sample size	Mutual exclusion was observed based on the comparison of all 94 Xt genomes available on NCBI. To obtain a comprehensive genomic dataset, one type or pathotype strain for each Xanthomonas species and pathovar possessing X-T4SS and/ or T6SS-i4 were used for comparative genetics and phylogenetic analyses.
Data exclusions	No data were excluded.
Replication	For all experiments presented all the results are replicable. This was verified through multiple replications of each experiment in different laboratories and by different experimentators.
Randomization	Not applicable. Randomization was considered as not relevant thanks to the different controls used.
Blinding	Not applicable. Blinding was considered as not relevant thanks to the different controls used.

Reporting for specific materials, systems and methods

We require information from authors about some types of materials, experimental systems and methods used in many studies. Here, indicate whether each material, system or method listed is relevant to your study. If you are not sure if a list item applies to your research, read the appropriate section before selecting a response.

Materials & experimental systems

n/a	Involved in the study
☒	☐ Antibodies
☒	☐ Eukaryotic cell lines
☒	☐ Palaeontology and archaeology
☒	☐ Animals and other organisms
☒	☐ Clinical data
☒	☐ Dual use research of concern
☐	☒ Plants

Methods

n/a	Involved in the study
☒	☐ ChIP-seq
☒	☐ Flow cytometry
☒	☐ MRI-based neuroimaging

Plants

Seed stocks	Seed stocks of barley cv. Hercule were provided by the cereal and oilseed pilot centre CePiCOP (Gembloux).
Novel plant genotypes	No novel plant genotype was used.
Authentication	Authentication of seed stocks was ensured by the supplier.